Weierstraß-Institut
für Angewandte Analysis und Stochastik

Leibniz-Institut im Forschungsverbund Berlin e. V.

Preprint ISSN 2198-5855

Spinodal decomposition and collapse of a polyelectrolyte gel

Giulia L. Celora[1], Matthew G. Hennessy[1], Andreas Münch[1], Sarah L. Waters[1],

Barbara Wagner[2]

submitted: June 17, 2020

[1] Mathematical Institute
Andrew Wiles Building, Woodstock Road
Oxford, OX2 6GG
UK
E-Mail: celora@maths.ox.ac.uk
hennessy@maths.ox.ac.uk
muench@maths.ox.ac.uk
waters@maths.ox.ac.uk

[2] Weierstrass Institute
Mohrenstr. 39
10117 Berlin
Germany
E-Mail: barbara.wagner@wias-berlin.de

No. 2731
Berlin 2020

2010 *Mathematics Subject Classification.* 74A30, 80A22, 34B15.

2010 *Physics and Astronomy Classification Scheme.* 83.80.Rs, 83.10.Tv.

Key words and phrases. Polyelectrolyte gel, phase separation, collapse.

MH recognizes support from the Mathematical Institute through a Hooke fellowship, and GC acknowledges support through a Dphil scholarship from the SABS CDT, University of Oxford.

Edited by
Weierstraß-Institut für Angewandte Analysis und Stochastik (WIAS)
Leibniz-Institut im Forschungsverbund Berlin e. V.
Mohrenstraße 39
10117 Berlin
Germany

Fax: +49 30 20372-303
E-Mail: preprint@wias-berlin.de
World Wide Web: http://www.wias-berlin.de/

Spinodal decomposition and collapse of a polyelectrolyte gel

Giulia L. Celora, Matthew G. Hennessy, Andreas Münch, Sarah L. Waters,

Barbara Wagner

Abstract

The collapse of a polyelectrolyte gel in a (monovalent) salt solution is analysed using a new model that includes interfacial gradient energy to account for phase separation in the gel, finite elasticity and multicomponent transport. We carry out a linear stability analysis to determine the stable and unstable spatially homogeneous equilibrium states and how they phase separate into localized regions that eventually coarsen to a new stable state. We then investigate the problem of a collapsing gel as a response to increasing the salt concentration in the bath. A phase space analysis reveals that the collapse is obtained by a front moving through the gel that eventually ends in a new stable equilibrium. For some parameter ranges, these two routes to gel shrinking occur together.

1 Introduction

Ever since the seminal papers by Tanaka et al. [29] and Dusek [10] research on swelling and collapse of polyelectrolyte gels has been very intensive, both theoretically and experimentally [7, 6, 22, 23, 16]. The interest is on one hand grounded in the intriguing and subtle properties of such a system, combining elements of electrochemistry and condensed matter physics, on the other hand in its innumerable technological applications, where a better understanding of polyelectrolyte gels serves as a basis for developing smart, responsive materials and sensors [2, 5, 14, 28], for example. In particular, research in this field is driven by applications in medicine [14, 19], e.g. for drug delivery, tissue engineering, but also as a means of gaining fundamental insight into diverse phenomena in biology, where polyelectrolyte gels are used as a model system for many types of biological tissues [20, 24]. Polyelectrolytes also serve as a model for bio-macromolecules such as DNA, RNA [11, 32, 26].

In its simplest form a polyelectrolyte gel is a network of covalently cross-linked polyelectrolyte macromolecules, that is, of chains carrying fixed charges of the same sign, solved in a solute. If placed in a salt solution, the gel will approach a new equilibrium state attributed to osmotic effects and thereby swell or shrink. This process depends in a subtle way on the concentration and valency of the salt in the solvent, the pH value, the (nonlinear) elasticity of the gel, the concentration of fixed charges and the number of ionizable groups of the polyelectrolyte macromolecule, apart from the other external fields such a temperature or an applied electric field. It is typically described via a volume phase transition using thermodynamical equilibrium descriptions with jump conditions at interfaces between the co-existing phases [8, 15, 31] or variational methods. Unlike volume phase transitions in neutral hydrogels [13, 1, 9], subtle changes can have dramatic effects and moreover can result in discontinuous phase transitions connected with super-collapse [18, 17] and, in more recent studies, re-entrant swelling [27].

A deeper understanding of these phenomena, in particular when comparing to experiments, can be obtained if stability and the transient dynamics between equilibrium states can be resolved in order to

DOI 10.20347/WIAS.PREPRINT.2731 Berlin 2020

shed light on pattern forming processes leading to collapse [21, 33]. We use non-equilibrium thermodynamics to systematically derive a phase-field-type model of a polyelectrolyte gel that accounts for the free energy of the internal interfaces which form upon phase separation, as well as finite elasticity, multi-component transport via a Stefan-Maxwell together with a thermodynamically consistent model for the salt solution [4]. The main goal of this study is to systematically investigate the stability and the transient dynamics of this system by identifying the dominant parameters and time scales and analysing the respective asymptotic regimes, via stability analysis, phase space analysis and numerical simulations for the one-dimensional setting.

In section 2 we formulate the problem for the case of a one-dimensional constrained gel in contact with a bath of a salt solution and determine the dimensionless parameters that characterise the model. The distinctive ones for a poly-electrolyte as opposed to a neutral hydrogel are the ratio, β, of the Debye-length to the size of the gel; its ratio β/ω to the width of the interface between the swollen and the shrunk phase of the gel; and the ratio of the salt concentration in the bath and of the fixed charges on the polymer network, $\gamma = c_0/\alpha_f$. The electro-neutral limit corresponds to small β and we will typically also assume $\beta/\omega \ll 1$. The dilute limit, on the other hand, arises when γ is small, and as a consequence the concentration of positive mobile ions relative to the concentration of positive fixed charges in the gel, for example, is small.

In section 3 we carry out a stability analysis for the one-dimensional gel that maps out the stable and unstable homogeneous for the full model and also for various asymptotic limits of the aforementioned parameters. We also show numerically that in the unstable case, the nonlinear solutions form localized phase-separated regions with high and low concentration of the solvent, which eventually coarsen into the new stable gel state. Interestingly, in the low solvent regions there is a high ion (ϕ_-) concentration at each center of the dry patch, as a consequence of maintaining electro-neutrality.

In section 4 we numerically investigate the collapse of the gel by instantly switching the concentration of the ions in the bath, which leads to the change in concentration of the positive ions (ϕ_+) in the gel, which leads to the formation of a depletion front that propagates into the gel as the gel collapses into a new stable dry state. We systematically describe and characterize the states and the depletion front during collapse. In particular, we reveal via a phase-space analysis that the depletion front selects the homogeneous states in front and behind of it and these are always linearly stable.

Depending on the value of ϕ_+, the switching of the ion concentration is accompanied by a spinodal decomposition of the initial homogeneous state followed by coarsening of the localized concentration landscape, until eventually these regions are consumed by the intruding depletion front leaving behind a new stable homogeneous dry state. In section 5, we draw our conclusions and give an outlook on further research directions.

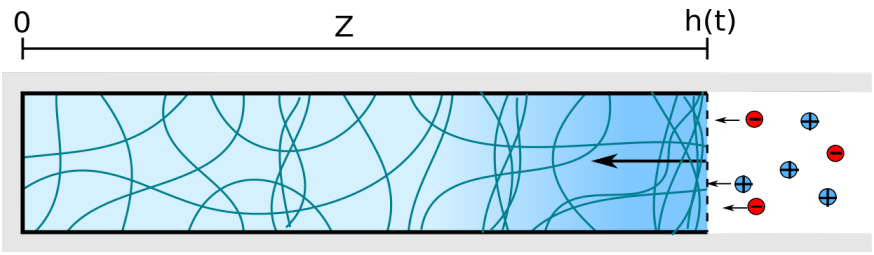

Figure 1: Schematic of the 1D setup

2 Formulation

Starting from the model derived in [4], we here consider the specific case of a polyelectrolyte gel swelling in a solution containing a monovalent salt. Consequently, we only need to consider two ionic species with charge $z_+ = 1$ and $z_- = -1$. Under this condition, the dynamics of the system in an Eulerian coordinate system is governed by the following set of equations:

$$\partial_t c_s + \nabla \cdot (c_s \boldsymbol{v}_n) = -\nabla \cdot \boldsymbol{j}_s, \tag{1a}$$

$$\partial_t c_\pm + \nabla \cdot (c_\pm \boldsymbol{v}_n) = \nabla \cdot \left[\frac{\mathcal{D}_\pm c_\pm}{k_B T} \nabla \mu_\pm - \frac{\mathcal{D}_\pm c_\pm}{\mathcal{D}_\pm^0 c_s} \boldsymbol{j}_s \right], \tag{1b}$$

$$\nabla \cdot \mathbf{T} = 0, \tag{1c}$$

$$-\epsilon \nabla^2 \Phi = e \left(z_f c_f + z_+ c_+ + z_- c_- \right), \tag{1d}$$

The first equation is for the conservation of solvent, followed by the conservation of the two mobile species in conjunction with a linear law for the the diffusive fluxes of these species in terms of the gradient of the chemical potentials. The constitutive laws in this model are chosen to be thermodynamically consistent following the approach by Gurtin [12]. The third equation is simply conservation of momentum in the quasi-static approximation. Finally, we have the law of electrostatics giving the electrical potential generated by the mobile charges as well as the charges fixed to the polyelectrolyte chains, in the presence of a homogeneous dielectric medium. Moreover, to complete the model, we need further constitutive laws, starting with a linear law for the diffusive flux of the solvent,

$$\boldsymbol{j}_s = -c_s \mathcal{K} \left(\nabla \mu_s + \sum_{i=+,-} \frac{c_i \mathcal{D}_i}{c_s \mathcal{D}_i^0} \nabla \mu_i \right), \tag{2a}$$

and expressions for the three chemical potentials

$$\mu_s = p v_s + \mu_s^0 - \gamma \nabla^2 c_s + k_B T \left[\ln(c_s v_s) + 1 + \frac{\chi (1 - c_s v_s)}{J} - \sum_m c_m v_s \right], \tag{2b}$$

$$\mu_\pm = p v_\pm + \mu_\pm^0 + z_\pm e \Phi + k_B T \left[\ln(v_\pm c_\pm) + 1 - \sum_{m=s,+,-} v_\pm c_m - \frac{\chi c_s v_\pm}{J} \right]. \tag{2c}$$

For the stresses in the elastic network, we have four contributions

$$\mathbf{T} = -p\mathbf{I} + \mathbf{T}^{kort} + \mathbf{T}^{Max} + \frac{G(\mathbf{B} - \mathbf{I})}{J}. \tag{2d}$$

The first and last are the isotropic stress induced by the pressure and the elastic response of a neo-Hookean polymer network, respectivel, while the other two represent the Korteweg stress generated at internal interfaces (i.e., gradients of the solvent concentration)

$$\mathbf{T}^{Kort} = \gamma \left[\left(\frac{|\nabla c_s|^2}{2} + c_s \nabla^2 c_s \right) \mathbf{I} - \nabla c_s \otimes \nabla c_s \right], \tag{2e}$$

and the Maxwell stresses due to the presence of electric charges,

$$\mathbf{T}^{Max} = \epsilon \left[\nabla \Phi \otimes \nabla \Phi - \frac{1}{2} |\nabla \Phi|^2 \mathbf{I} \right]. \tag{2f}$$

The variable J represents the volume expansion of the gel compared to the dry reference state, where $J = 1$. In the general situation, it can be expressed in terms of the inverse volume fraction of the network, or, if written in terms of the solvent and ion species,

$$J = \left(1 - v_s c_s - v_+ c_+ - v_- c_-\right)^{-1}. \tag{3}$$

The notation is as follows: The Eulerian coordinates are $\boldsymbol{x} = (x, y, z)$, t is time, c_s, c_+ and c_-, and c_f are the concentration (number of molecules per volume) of the solvent, positive and negative mobile ionic species, and of the fixed charges, respectively, while μ_s, μ_+ and μ_- denote the chemical potentials associated with each of these species, v_s, v_+ and v_- are the respective volumes per molecule, and $\boldsymbol{j}_s$, $\boldsymbol{j}_+$, $\boldsymbol{j}_-$ are the corresponding fluxes. The potential of the electric field is denoted by Φ. Also, the tensor $\mathbf{B} = \mathbf{F}\mathbf{F}^T$ is the left Cauchy-Green tensor, and $\mathbf{F} = \partial \boldsymbol{x}/\partial \boldsymbol{X}$ the deformation strain tensor with determinant J, where $\boldsymbol{X}$ are the Lagrangian coordinates. Moreover, $\boldsymbol{v}_n = \partial \boldsymbol{X}/\partial \boldsymbol{t}$ is the velocity of the polymer network. Our reference system pertains to the dry state of the gel. The parameters are ϵ for the absolute permittivity of the gel (which is assumed to be constant), $\mathcal{D}_s$ and $\mathcal{D}_\pm$ are the diffusion coefficients of the solvent and the mobile ions in the gel, and $\mathcal{D}_\pm^0$ are the diffusivities of the ionic species in the pure solvent. The coefficient γ plays the role of the surface energy. The parameters μ_S^0, $\mu_\pm^0$ denote the chemical potential of the non-interacting solvent and ionic species. Young's modulus for the gel network is given by G, and χ is the Flory-Huggins parameter characterising the solvent-network interaction.

As commonly assumed in the study of ionic solution, we here consider the specific case of equal molecular volume for all of the mobile species considered $v = v_s = v_+ = v_-$. We here assume that the friction between the different ion species and of ions with the gel is negligible compared to the dissipation due to the relative motion between the ions and the solvent. Thus we can simplify the model assuming $\mathcal{D}_\pm = \mathcal{D}_\pm^0$. Given this, the parameter $\mathcal{K}$ reduces to the permeability coefficient for the flow of the pure solvent in a poro-elastic material, for which we have the law

$$\mathcal{K} = \frac{\mathcal{D}_s \phi_n^\theta}{k_B T}, \tag{4}$$

where $\phi_n = (1 - v_s c_s - v_+ c_+ - v_- c_-)$ is the volume fraction of the polymer network and the exponent $\theta = -1.5$ has been estimated from experimental observations of hydrogels (see e.g. [9] and references therein), and $\mathcal{D}_s$ is . . ..

Moreover, we assume that the number of sites of the fixed charges per unit volume is C_f, so that in the current state, the number density is

$$c_f = C_f \phi_n. \tag{5}$$

Constrained Swelling

In this work, we focus on the dynamics of a constrained gel which undergoes uni-axial deformation due to the uptake or release of a solution. In this condition the deformation tensor $\mathbf{F}$ is of the form:

$$\mathbf{F} = \begin{bmatrix} 1 & 0 & 0 \\ 0 & 1 & 0 \\ 0 & 0 & J(z,t) \end{bmatrix}. \tag{6}$$

Before moving on with our analysis, we non-dimensionalise the system (1)-(3) and assume all of the model variables to depend only on z and t:

$$\mu_m^* = \frac{\mu_m - \mu_m^0 + T_0 v}{k_B T}, \qquad \phi_m = v c_m, \qquad \phi_f = v c_f, \quad \Phi^* = \frac{\Phi e}{k_B T}, \tag{7}$$

$$\mathbf{T}^* = \frac{\mathbf{T}}{G}, \qquad z^* = \frac{z}{L}, \qquad t^* = \frac{t}{\tau}, \qquad Q^* = \frac{Qv}{e}, \tag{8}$$

$$p^* = \frac{p + T_0}{G}, \qquad j_m^* = \frac{vL}{\mathcal{D}_s} j_m, \qquad \tau = \frac{L^2}{\mathcal{D}_s} \tag{9}$$

where L is the characteristic size of the gel, and $m = s, +, -$. By integrating the one-dimensional version of the stress balance (1c) in the vertical direction, we obtain that the T_{zz}-component of the stress tensor is spatially homogeneous but may be time dependent, $T_{zz} = T_0(t)$. Dropping the star notation, the non-dimensional problem formulation reads:

$$\partial_t \phi_s + \partial_z(\phi_s v_n) = -\partial_z j_s, \tag{10a}$$

$$\partial_t \phi_\pm + \partial_z(\phi_\pm v_n) = -\partial_z j_\pm, \tag{10b}$$

$$-\beta^2 \partial_{zz}\Phi = z_+\phi_+ + z_-\phi_- + \alpha_f \phi_n \tag{10c}$$

$$p = \frac{\omega^2}{\mathcal{G}}\left[\phi_s \partial_{zz}\phi_s - \frac{(\partial_z \phi_s)^2}{2}\right] + \frac{\beta^2}{2\mathcal{G}}\left(\partial_z \Phi\right)^2 + \frac{(1-\phi_n^2)}{\phi_n} \tag{10d}$$

where

$$j_s = -\phi_s \phi_n^\theta \left(\partial_z \mu_s + \sum_{i=+,-} \frac{\phi_i}{\phi_s} \partial_z \mu_i\right), \tag{11a}$$

$$j_\pm = -\mathcal{D}_\pm \phi_\pm \partial_z \mu_\pm + \frac{\phi_\pm}{\phi_s} j_s, \tag{11b}$$

$$\mu_s = p\mathcal{G} - \omega^2 \partial_{zz}\phi_s + \ln \phi_s + \left[\chi(1-\phi_s) + 1\right]\phi_n, \tag{11c}$$

$$\mu_\pm = p\mathcal{G} + z_\pm \Phi + \ln(\phi_\pm) + \left[1 - \chi\phi_s\right]\phi_n, \tag{11d}$$

$$v_n = -j_s - j_+ - j_-, \tag{11e}$$

$$\phi_n = 1 - \phi_s - \phi_+ - \phi_-. \tag{11f}$$

For the boundary conditions, we assume that the gel is bounded by a substrate or wall at $z = 0$ and is in contact with a bath at $z = h(t)$. At $z = 0$, we therefore impose no-flux boundary conditions for all species and assume a neutral wall, so that we have a special case of the conditions used in surface-directed phase separation [25]. Hence

$$j_s = 0, \quad j_+ = 0, \tag{12a}$$

$$\partial_z \phi_s = 0. \tag{12b}$$

We put the gel in contact with a bath that contains a salt solution at concentration c_0 far away from the interface, that is, the number of each of the mobile ion species per volume. At the interface with the bath, $z = h(t)$, we have to impose the following boundary conditions resulting from the Debye layer

analysis in [3]. These are

$$\partial_z \phi_s = 0, \tag{13a}$$

$$\omega^2 \left(1-\phi_s\right)\partial_{zz}\phi_s = \mathcal{G}\frac{1-\phi_n^2}{\phi_n} + \left(\chi(1-\phi_s)+1\right)\phi_n + \ln\frac{\phi_s}{1-2c_0}, \tag{13b}$$

$$\phi_+ = c_0 \exp\left[-\Phi - \mathcal{G}p - \left(1-\chi\phi_s\right)\phi_n\right], \tag{13c}$$

$$\Phi = \sinh^{-1}\left[\frac{\alpha_f \phi_n}{2c_0}\exp\left(\mathcal{G}p + \phi_n\left(1-\chi\phi_s\right)\right)\right]. \tag{13d}$$

Finally we have a simple ODE describing the growth of the domain:

$$\frac{dh}{dt} = -\left(j_s + 2j_+\right)_{z=h(t)} \tag{13e}$$

The nondimensional equations shows that the system is characterised by three characteristic length scales L and

$$L_d = \sqrt{\frac{\epsilon k_B T v}{e^2}} \quad \text{and} \quad L_{int} = \sqrt{\frac{\gamma_0}{v k_B T}}, \tag{14}$$

that define the order of magnitude of the non-dimensional parameters

$$\beta = \frac{L_d}{L} \quad \text{and} \quad \omega = \frac{L_{int}}{L} \tag{15}$$

and are used to study the different asymptotic limits of the system. Further non-dimensional material parameters are

$$\mathcal{G} = \frac{vG}{k_B T}, \quad \mathcal{D}_\pm^* = \frac{\mathcal{D}_\pm}{\mathcal{D}_s}, \quad \text{and} \quad \alpha_f = z_f v C_f. \tag{16}$$

Depending on the application, different limits can be studied. For example, for the problem in [30] value for the known parameter $k_B = 1.38\times10^{-23}$, $T = 293K$, $e = 1.6\times10^{-19}C$ and $v = 3\times10^{-29}m^3$ and satisfy the following relation:

$$L_d \sim O(10^{-6}) \ll L, \quad L_d \ll L_{int} \Rightarrow \beta \ll \omega \tag{17}$$

In passing, we extract some useful scaling information from these boundary conditions, to set a scale for ϕ_+ when the salt concentration is very low, so that $c_0 \ll \alpha_f \ll 1$. Then the dominant terms in the argument of $\sinh^{-1}$ is the prefactor, so that $\Phi = \mathcal{O}(\alpha_f/c_0) \gg 1$. The Φ contribution will then dominate the argument of $\exp$ in (13c), so that we conclude

$$\phi_+ \sim c_0^2/\alpha_f. \tag{18}$$

For the analysis it is convenient to use the expression for the pressure (10d) and rewrite the chemical potentials in the following form:

$$\mu_s = F_s(\phi_s,\phi_+,\phi_-) + \frac{\beta^2}{2}\left(\partial_z\Phi\right)^2 + \left(\phi_s-1\right)\omega^2\partial_{zz}\phi_s - \omega^2\frac{\left(\partial_z\phi_s\right)^2}{2}, \tag{19a}$$

$$\mu_\pm = F_\pm(\phi_s,\phi_+,\phi_-) + \frac{\beta^2}{2}\left(\partial_z\Phi\right)^2 + z_\pm\Phi + \omega^2\phi_s\partial_{zz}\phi_s - \omega^2\frac{\left(\partial_z\phi_s\right)^2}{2}, \tag{19b}$$

where the functions F_+, F_- and F_s are defined as follows:

$$F_s = \mathcal{G}\frac{(1-\phi_n^2)}{\phi_n} + \ln\phi_s + \left[\chi(1-\phi_s)+1\right]\phi_n, \tag{19c}$$

$$F_\pm = \mathcal{G}\frac{(1-\phi_n^2)}{\phi_n} + \ln\phi_\pm + \left[1-\chi\phi_s\right]\phi_n. \tag{19d}$$

3 Stability analysis of the homogeneous states

Let us consider a perturbation around an originally homogeneous steady state $(\phi_s, \phi_\pm, \Phi) = (\bar{\phi}_s, \bar{\phi}_\pm, \bar{\Phi})$, of the system (10)-(19)which, as shown in our previous works needs to satisfy the electro-neutrality condition [4]:

$$z_+\bar{\phi}_+ + z_-\bar{\phi}_- + \alpha_f\bar{\phi}_n = 0, \quad \alpha_f = vC_f. \tag{20}$$

Assuming periodic boundary condition, we have the following ansatz for the form of the normal modes:

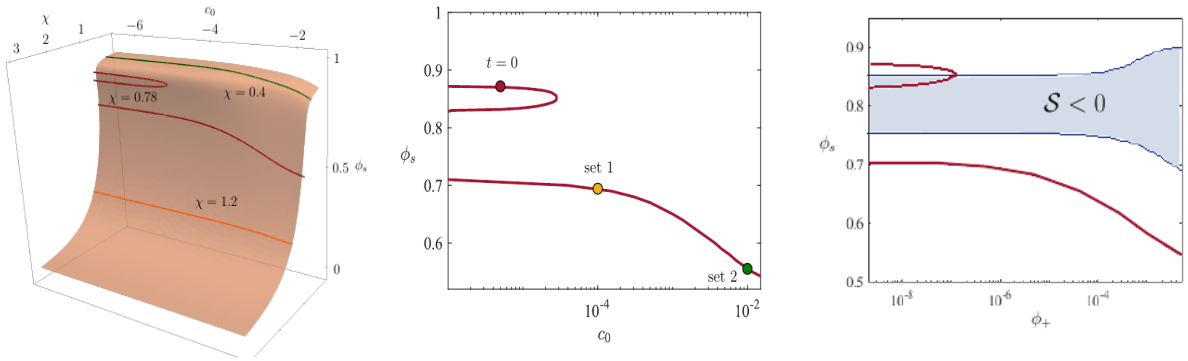

Figure 2: Analysis of the dependency of the equilibrium on the ions concentration in the bath c_0. In (a) we compute the equilibrium manifold in the phase diagram (c_0, χ, ϕ_s). We here consider parameter as in Table 1 with c_0, used as a control parameter, is allowed to vary between $[2\times10^{-6}, 2\times10^{-2}]$. The curve are section of the manifold taken for specific values of the χ parameter. We can see that as χ increase the system undergoes a bifurcation, switching for a single highly swollen state, to a transient bi-stable regime. Finally for sufficiently high χ, the collapsed state is the only steady state of the system. In (b)-(c) we further analyse the bistable regime. In (b) we show the equilibrium curve $(c_0, \phi_s(c_0))$, while in (b) the curve $(\phi_+(c_0), \phi_s(c_0))$ to compare it with the region of linear instability (highlighted in blue). As we can see the model present a "Pitchfork bifurcation". At low c_0 the only steady state is characterised by low concentration of solvent, i.e. collapsed state; as we increase the concentration an additional disconnected branch appears, which is characterised by two highly swollen steady state, a stable and an unstable one (as shown in (c) the middle equilibrium lies in the linearly unstable region predicted in this section). As shown in Figure (b) for the simulation in Section, we start on the stable upper branch of the equilibrium curve at low c_0. By increasing the c_0 we are able to drive the system to a collapsed state on the lower branch.

$$\begin{aligned} \phi_s = \bar{\phi}_s + \delta\phi_s^* e^{ikz+\lambda t}, \quad \phi_\pm = \bar{\phi}_\pm + \delta\phi_\pm^* e^{ikz+\lambda t}, \quad \Phi = \bar{\Phi} + \delta\Phi^* e^{ikz+\lambda t} \\ j_s = -ik\delta j_s^* e^{ikz+\lambda t}, \quad j_\pm = -ik\delta j_\pm^* e^{ikz+\lambda t}. \end{aligned} \tag{21}$$

where * denotes perturbation functions and δ the amplitude of the perturbation. By substituting into the model and considering only the linear term in the equation, we obtain:

$$\lambda\phi_s^* + k^2\left[\left(1-\bar{\phi}_s\right)j_s^* - \bar{\phi}_s j_+^* - \bar{\phi}_s j_-^*\right] = 0, \tag{22a}$$
$$\lambda\phi_+^* + k^2\left[\left(1-\bar{\phi}_+\right)j_+^* - \bar{\phi}_+ j_-^* - \bar{\phi}_+ j_s^*\right] = 0, \tag{22b}$$
$$\lambda\phi_-^* + k^2\left[\left(1-\bar{\phi}_-\right)j_-^* - \bar{\phi}_- j_+^* - \bar{\phi}_- j_s^*\right] = 0, \tag{22c}$$
$$\beta^2k^2\Phi^* = \left(z_+ - \alpha_f\right)\phi_+^* + \left(z_- - \alpha_f\right)\phi_-^* - \alpha_f\phi_s^*, \tag{22d}$$
$$j_s^* = \bar{\phi}_n^\theta\left[\sum_\ell\sum_m \bar{\phi}_m\frac{\partial F_m}{\partial\phi_\ell}\phi_\ell^* + k^2\omega^2\bar{\phi}_s\bar{\phi}_n\phi_s^* - \alpha_f\bar{\phi}_n\Phi^*\right], \tag{22e}$$
$$j_+^* - \frac{\bar{\phi}_+}{\bar{\phi}_s}j_s^* = \mathcal{D}_+\bar{\phi}_+\left[\sum_\ell\frac{\partial F_+}{\partial\phi_\ell}\phi_\ell^* + z_+\Phi^* - \omega^2k^2\bar{\phi}_s\phi_s^*\right], \tag{22f}$$
$$j_-^* - \frac{\bar{\phi}_-}{\bar{\phi}_s}j_s^* = \mathcal{D}_-\bar{\phi}_-\left[\sum_\ell\frac{\partial F_-}{\partial\phi_\ell}\phi_\ell^* + z_-\Phi * -\omega^2k^2\bar{\phi}_s\phi_s^*\right], \tag{22g}$$

where we have kept only the linear terms in the perturbations. Let us consider the case of a monovalent salt, i.e. $z_+ = 1$ and $z_- = -1$, with ions of equivalent diffusivity $\mathcal{D}_+ = \mathcal{D}_- = \mathcal{D}$. Imposing that the above linear system has non trivial solution, i.e. its determinant is zero, we obtain a third order equation in λ of the form:

$$-\beta^2 k^2 \lambda^3 + \frac{k^2\lambda^2}{\bar{\phi}_s} a_2 + \frac{\mathcal{D}k^4\lambda}{\bar{\phi}_s} a_1 + \mathcal{D}^2 k^6 \bar{\phi}_- \bar{\phi}_+ \bar{\phi}_n^{\theta+1} a_0 = 0, \tag{23}$$

where the coefficients a_2, a_1 and a_0 are functions of the steady state variables as well as the modes wavelength k and β. However, note that these are generally non-zero for $\beta \to 0$. Given the complexity of the model, it is difficult to tackle (23) for this reason we consider some limiting cases, which reflect condition usually encountered in actual gels.

3.1 The electro-neutral limit $\beta \ll 1$

Let us consider the limiting case of an electro-neutral gel, which emerges from the case $\beta \to 0$ [3]. Given that the limit admit a regular expansion, we can straightforwardly compute the leading order approximation of (22) setting $\beta = 0$. If we only consider the case $\alpha_f > 0$, then it is convenient to express the solution in terms of ϕ_+, and use Eqn. (22d) to eliminate ϕ_- so as to reduce the problem dimension. Further using a linear combination of Equations (22a)-(22c) we obtain the following condition on j_+^* and j_-^*:

$$j_-^* = -\frac{z_+}{z_-} j_+^*. \tag{24}$$

Substituting the definition of the fluxes (22g)-(22f), we also obtain an explicit algebraic equation for Φ^*:

$$\Phi^* = -\frac{1}{z_-}\left[\sum_{i=s,+} \frac{\partial F_-}{\partial \phi_i}\phi_i^* - k^2\omega^2\bar{\phi}_s\phi_s^* + \frac{z_+ j_+^*}{\mathcal{D}_- z_- \bar{\phi}_-} + \frac{j_s^*}{\mathcal{D}_-\bar{\phi}_s}\right]. \tag{25}$$

Using all of the above, we can thus reduce the original system (22) to the following system of four equations:

$$\lambda\phi_s^* + k^2\left[\left(1-\bar{\phi}_s\right) j_s^* + \frac{z_+ - z_-}{z_-}\bar{\phi}_s j_+^*\right] = 0, \tag{26a}$$

$$\lambda\phi_+^* + k^2\left[\left(1 + \frac{z_+ - z_-}{z_-}\bar{\phi}_+\right) j_+^* - \bar{\phi}_+ j_s^*\right] = 0, \tag{26b}$$

$$\left(1 - \frac{\alpha_f\bar{\phi}_n^{\theta+1}}{z_-\mathcal{D}_-\bar{\phi}_s}\right) j_s^* - \frac{\alpha_f\bar{\phi}_n z_+\bar{\phi}_n^{\theta}}{z_-^2\mathcal{D}_-\bar{\phi}_-} j_+^* = \tag{26c}$$

$$\bar{\phi}_n^{\theta}\left[\sum_{i=s,+}\left(\bar{\phi}_s a_{si} + \bar{\phi}_+ a_{+i}\right)\phi_i^* + k^2\omega^2\bar{\phi}_s\left(1 - \bar{\phi}_s - \bar{\phi}_+ + \frac{z_+}{z_-}\bar{\phi}_+\right)\phi_s^*\right]$$

$$\left(1 + \frac{\mathcal{D}_+ z_+^2\bar{\phi}_+}{\mathcal{D}_- z_-^2\bar{\phi}_-}\right) j_+^* \frac{\bar{\phi}_+}{\bar{\phi}_s}\left(1 - \frac{\mathcal{D}_+ z_+}{\mathcal{D}_- z_-}\right) j_s^* = \tag{26d}$$

$$\mathcal{D}_+\bar{\phi}_+\left[\sum_{i=s,+} a_{+i}\phi_i^* - k^2\omega^2\bar{\phi}_s\left(1 - \frac{z_+}{z_-}\right)\phi_s^*\right]$$

where we have introduced

$$a_{si} = \frac{\partial F_s}{\partial \phi_i}(\bar{\boldsymbol{\phi}}) + \frac{\partial F_s}{\partial \phi_-}(\bar{\boldsymbol{\phi}})\frac{\partial \bar{\phi}_-}{\partial \bar{\phi}_i}, \tag{27a}$$

$$a_{+i} = \frac{\partial \left(F_+ - \frac{z_+}{z_-}F_-\right)}{\partial \phi_i}(\bar{\boldsymbol{\phi}}) + \frac{\partial \left(F_+ - \frac{z_+}{z_-}F_-\right)}{\partial \phi_-}(\bar{\boldsymbol{\phi}})\frac{\partial \bar{\phi}_-}{\partial \bar{\phi}_i}. \tag{27b}$$

As for the full model, let us simplify the model considering the case of a monovalent salt, i.e. $z_+ = 1$ and $z_- = -1$, with equal diffusivity of the ions, i.e. $\mathcal{D}_+ = \mathcal{D}_-$ so that the system reduces to:

$$\lambda\phi_s^* + k^2\left[\left(1-\bar{\phi}_s\right)j_s^* - 2\bar{\phi}_s j_+^*\right] = 0, \tag{28a}$$

$$\lambda\phi_+^* + k^2\left[\left(1-2\bar{\phi}_+\right)j_+^* - \bar{\phi}_+ j_s^*\right] = 0, \tag{28b}$$

$$\begin{aligned}\left(1+\frac{\alpha_f\bar{\phi}_n^{\theta+1}}{\mathcal{D}\bar{\phi}_s}\right)j_s^* - \frac{\alpha_f\bar{\phi}_n^{\theta+1}}{\mathcal{D}\bar{\phi}_-}j_+^* = \bar{\phi}_n^\theta\left[\left(\bar{\phi}_s a_{s+} + \bar{\phi}_+ a_{++}\right)\phi_+^*\right.\\ \left.\left(\omega^2k^2\bar{\phi}_s\left(1+\alpha_f\right)\bar{\phi}_n + \bar{\phi}_s a_{ss} + \bar{\phi}_+ a_{+s}\right)\phi_s^*\right]\end{aligned} \tag{28c}$$

$$\left(1+\frac{\bar{\phi}_+}{\bar{\phi}_-}\right)j_+^* - \frac{2\bar{\phi}_+}{\bar{\phi}_s}j_s^* = \mathcal{D}\bar{\phi}_+\left[\left(a_{+s} - 2\omega^2k^2\bar{\phi}_s\right)\phi_s^* + a_{++}\phi_+^*\right]. \tag{28d}$$

In this case the explicit forms of the coefficients a_{ij}:

$$a_{ss} = \frac{\mathcal{G}\bar{\phi}_n^{-2}(\bar{\phi}_n^2+1) - 1 + \chi(\bar{\phi}_s - 1)}{1+\alpha_f} + \bar{\phi}_s^{-1} - \chi\bar{\phi}_n, \tag{29a}$$

$$a_{s+} = 2\,\frac{\mathcal{G}\bar{\phi}_n^{-2}(\bar{\phi}_n^2+1) - 1 + \chi(\bar{\phi}_s - 1)}{1+\alpha_f}, \tag{29b}$$

$$a_{+s} = \frac{2}{1+\alpha_f}\left(\mathcal{G}\bar{\phi}_n^{-2}(\bar{\phi}_n^2+1) + \chi\bar{\phi}_s - 1 - \frac{\alpha_f}{2\left(\bar{\phi}_+ + \alpha_f\bar{\phi}_n\right)}\right) - 2\chi\bar{\phi}_n, \tag{29c}$$

$$a_{++} = \frac{4}{1+\alpha_f}\left(\mathcal{G}\bar{\phi}_n^{-2}(\bar{\phi}_n^2+1) + \chi\bar{\phi}_s - 1 + \frac{1-\alpha_f}{4\left(\bar{\phi}_+ + \alpha_f\bar{\phi}_n\right)}\right) + \bar{\phi}_+^{-1}. \tag{29d}$$

Imposing the system to have non trivial solution, we obtain a quadratic equation that defined the modes λ. Using the general form:

$$\alpha_1\lambda^2 + \alpha_2k^2\lambda + k^4\alpha_3 = 0, \tag{30}$$

where the coefficients are defined as:

$$\alpha_1 = \frac{\bar{\phi}_s \mathcal{D}\left(2\bar{\phi}_+ + \alpha_f \bar{\phi}_n\right) + \alpha_f^2 \phi_n^{\theta+2}}{\mathcal{D}\bar{\phi}_s(\bar{\phi}_+ + \alpha_f \bar{\phi}_n)}, \tag{31}$$

$$\alpha_3 = \mathcal{D}\bar{\phi}_n^{\theta+1}\bar{\phi}_+\bar{\phi}_s\left(1+\alpha_f\right)\left[k^2\omega^2\left(a_{++}\left(1-\bar{\phi}_s\right)+2a_{s+}\bar{\phi}_s\right)+ (a_{++}a_{ss}-a_{s+}a_{+s})\right] \tag{32}$$

$$\begin{aligned}\alpha_2 = \omega^2 k^2 \bar{\phi}_s \bar{\phi}_n^{\theta+1}&\left(\frac{2\bar{\phi}_+\bar{\phi}_n\left(1+\alpha_f^2\right)+\bar{\phi}_n^2\alpha_f\left(1+\alpha_f\right)^2}{\bar{\phi}_+ + \alpha_f\bar{\phi}_n} + 4\frac{\mathcal{D}\bar{\phi}_s\bar{\phi}_+}{\bar{\phi}_n^{\theta+1}}\right) \\ &+a_{ss}\bar{\phi}_n^{\theta}\bar{\phi}_s\left(-4\bar{\phi}_+ + \frac{(1-\bar{\phi}_s)(2\bar{\phi}_+ + \alpha_f\bar{\phi}_n)}{\bar{\phi}_+ + \alpha_f\bar{\phi}_n}\right) \\ +a_{s+}\bar{\phi}_n^{\theta+1}\bar{\phi}_+&\frac{2\bar{\phi}_+ + \alpha_f + \alpha_f\left(1+\alpha_f\right)\bar{\phi}_n}{\bar{\phi}_+ + \alpha_f\bar{\phi}_n} + 2a_{+s}\bar{\phi}_+\left[\bar{\phi}_n^{\theta+1} - \bar{\phi}_s\mathcal{D}\right] \\ &+a_{++}\bar{\phi}_+\left[\mathcal{D}\left(1-2\bar{\phi}_+\right) + \frac{\bar{\phi}_n^{\theta+1}}{\bar{\phi}_s}\left(2\bar{\phi}_+ + \alpha_f\right)\right]\end{aligned} \tag{33}$$

Consequently we have that the system is stable if and only if:

$$\alpha_2 > 0, \quad \alpha_1\alpha_3 > 0. \tag{34}$$

Note that $\alpha_2 = \alpha_2(k)$ is a quadratic function of k with minimum at $k = 0$. Consequently the homogeneous steady state is stable whenever $\alpha_2(0) > 0$. Since also the coefficient α_1 is always positive, the second condition reduces to $\alpha_3(k) > 0$:

$$\omega^2 k^2 \bar{\phi}_s\left(a_{++}\left(1-\bar{\phi}_s\right)+2a_{s+}\bar{\phi}_s\right) + \left(a_{++}a_{ss} - a_{s+}a_{+s}\right)\bar{\phi}_s > 0, \tag{35}$$

for any k. Again (35) is a quadratic function in k (with vertex at $k = 0$), so that the system is stable if the curvature is positive and its minimum at $k = 0$ is positive. The stability region is thus defined by the following set of inequalities:

$$a_{++}\left(1-\bar{\phi}_s\right) + 2a_{s+}\bar{\phi}_s > 0 \tag{36a}$$

$$a_{++}a_{ss} - a_{s+}a_{+s} > 0 \tag{36b}$$

$$\begin{aligned}a_{ss}\bar{\phi}_n^{\theta+1}\bar{\phi}_s&\frac{2\bar{\phi}_+ + \alpha_f\bar{\phi}_n\left(1+\alpha_f\right)}{\bar{\phi}_+ + \alpha_f\bar{\phi}_n} \\ +a_{s+}\bar{\phi}_n^{\theta+1}\bar{\phi}_+&\frac{2\bar{\phi}_+ + \alpha_f + \alpha_f\left(1+\alpha_f\right)\bar{\phi}_n}{\bar{\phi}_+ + \alpha_f\bar{\phi}_n} + 2a_{+s}\bar{\phi}_+\left[\bar{\phi}_n^{\theta+1} - \bar{\phi}_s\mathcal{D}\right] \\ &+a_{++}\bar{\phi}_+\left[\mathcal{D}\left(1-2\bar{\phi}_+\right) + \frac{\bar{\phi}_n^{\theta+1}}{\bar{\phi}_s}\left(2\bar{\phi}_+ + \alpha_f\right)\right] > 0\end{aligned} \tag{36c}$$

There are several degrees of freedom in the model. We here set the values of the parameters $\mathcal{G}$, α_f, $\mathcal{D}$ and θ as for the numerical simulations presented in the next section (see Table 1). We further consider $\bar{\phi}_+$ as a control parameter and investigate for different value of the latter the change in the stability region in the plane $(\bar{\phi}_s, \chi)$. For the set of parameter here considered we have that the stability region is bounded by the curve:

$$\mathcal{S}(\phi_s, \phi_+, \chi) = a_{11}a_{22} - a_{12}a_{21} = 0. \tag{37}$$

The latter is illustrated in Figure 3. As (a) remains positive, the term related to the interface energy in (35) helps with the stabilization of the system. In particular we have that there exist a value $k^*(\omega; \bar{\phi}_s, \chi)$ which is an upper bound for the unstable nodes. As $\omega \to 0$ we have that the $k^* \to \infty$ so that all modes are unstable. In order for such instabilities to develop, the characteristic length of the gel needs to be greater than $\lambda^* = 2\pi/k^*$ which in an increasing function of ω and $\lambda^* \to 0$ for $\omega \to 0$.

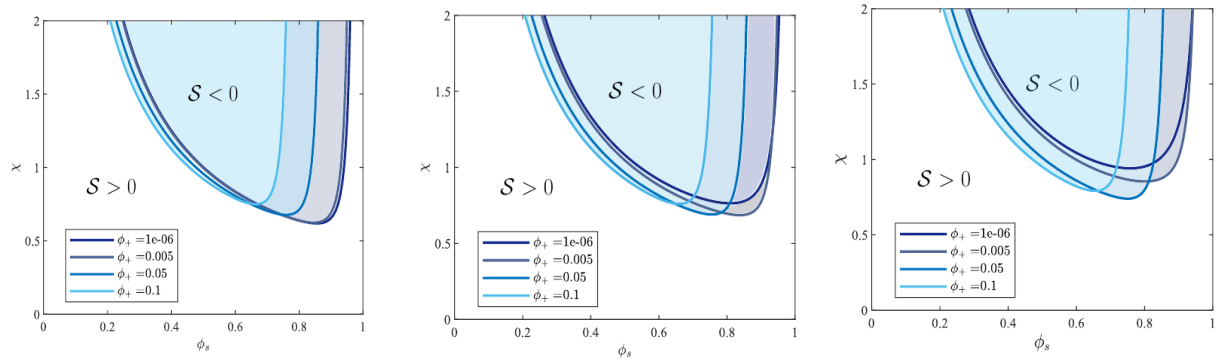

(a) $\alpha_f = 0$ **(b)** $\alpha_f = 0.04$ **(c)** $\alpha_f = 0.1$

Figure 3: Effect of $\bar{\phi}_+$ on the stability of the electro-neutral model. As expected for small value of the parameter there are small changes to the stability region of the system. However, we see that higher concentration of fixed charged, α_f, tend to stabilise the system moving the unstable region up. This will be further investigate in what follow. On the other hand, when $\bar{\phi}_+$ is of the same order as $\bar{\phi}_s$ we have a non-negligible shift of the stability region toward the left, which seems to be independent of the value α_f. The other parameters, i.e. $\mathcal{G}$, $\mathcal{D}$ and θ are taken from Table 1.

3.1.1 The dilute sublimit $\phi_+ \ll 1$ for $\beta \ll \omega \ll 1$

Let us further simplify the model considering the dilute limit, i.e. $\xi = \bar{\phi}_+ << \bar{\phi}_s$. Unlike for the electro-neutral limit, we now have a singular perturbation, due to the contribution of $a_{++}\, O(\xi^{-1})$. For this reason, we present a more detailed derivation of this limit. Not also that we allow $\bar{\phi}_-$ (and thus the fix charges) to be non-dilute, so to capture also the case of a collapse gel with higher concentration of fixed charges. Consequently we have that at the volume fractions for the network and the negative ions can be written as:

$$\bar{\phi}_n = \frac{1-\bar{\phi}_s}{1+\alpha_f} - \frac{2\xi}{1+\alpha_f} = \bar{\phi}_n^{(0)} - \frac{2\xi}{1+\alpha_f}, \tag{38}$$

$$\bar{\phi}_- = \alpha_f \bar{\phi}_n^{(0)} + \frac{1-\alpha_f}{1+\alpha_f}\xi. \tag{39}$$

To start with, we look at the form of the functions a_{ij} under this assumption. We can infer

$$a_{ss} \sim \mathcal{G}\frac{(\bar{\phi}_n^{(0)})^2+1}{\bar{\phi}_n^{(0)}\left(1-\bar{\phi}_s\right)} - \frac{1}{1+\alpha_f} - 2\chi\bar{\phi}_n^{(0)} + \bar{\phi}_s^{-1} + O(\xi), \tag{40a}$$

$$a_{s+} \sim 2\,\mathcal{G}\frac{(\bar{\phi}_n^{(0)})^2+1}{\bar{\phi}_n^{(0)}\left(1-\bar{\phi}_s\right)} - \frac{2}{1+\alpha_f} - 2\chi\bar{\phi}_n^{(0)} + O(\xi) \tag{40b}$$

$$a_{+s} \sim 2\,\mathcal{G}\frac{(\bar{\phi}_n^{(0)})^2+1}{\bar{\phi}_n^{(0)}\left(1-\bar{\phi}_s\right)} + \frac{2\chi(2\bar{\phi}_s-1)}{1+\alpha_f} - \frac{2}{1+\alpha_f} - \frac{1}{1-\bar{\phi}_s} + O(\xi), \tag{40c}$$

$$a_{++} = \frac{1}{\xi} + 4\,\mathcal{G}\frac{(\bar{\phi}_n^{(0)})^2+1}{\bar{\phi}_n^{(0)}\left(1-\bar{\phi}_s\right)}\frac{4\left(\chi\bar{\phi}_s-1\right)}{1+\alpha_f} + \frac{(1-\alpha_f)}{\alpha_f(1-\bar{\phi}_s)} + O(\xi). \tag{40d}$$

Let us now denote with $a_{ij}^{(n)}$ the component of the coefficient which is of order $O(\xi^n)$. Then the first order approximation of the modes $\lambda^{(0)}$ is defined by the quadratic equation:

$$\alpha_1^{(0)}(\lambda^{(0)})^2 + \alpha_2^{(0)}k^2\lambda^{(0)} + k^4\alpha_3^{(0)} = 0, \tag{41}$$

with coefficients

$$\alpha_1^{(0)} = 1 + \frac{\alpha_f(\bar{\phi}_n^{(0)})^{\theta+1}}{\mathcal{D}\bar{\phi}_s}, \tag{42a}$$

$$\alpha_2^{(0)} = \omega^2 k^2 \bar{\phi}_s(\bar{\phi}_n^{(0)})^{\theta+2}(1+\alpha_f)^2 + a_{ss}^{(0)}(\bar{\phi}_n^{(0)})^{\theta}\bar{\phi}_s(1-\bar{\phi}_s) + \xi a_{++}^{(-1)}\left[\mathcal{D} + \frac{\alpha_f(\bar{\phi}_n^{(0)})^{\theta+1}}{\bar{\phi}_s}\right] \tag{42b}$$

$$\alpha_3^{(0)} = \mathcal{D}(\bar{\phi}_n^{(0)})^{\theta+1}\bar{\phi}_s\xi\,(1+\alpha_f)\left[k^2\omega^2 a_{++}^{(-1)}\left(1-\bar{\phi}_s\right) + a_{++}^{(-1)}a_{ss}^{(0)}\right]. \tag{42c}$$

It is now apparent that the terms in ω^2 are positive and thus enhance the stability of the system and the homogenous state is unstable if the condition $\mathcal{S} = \bar{\phi}_s a_{ss}^{(0)} < 0$ is fulfilled:

$$\mathcal{S} = 1 - \frac{\bar{\phi}_s\left[1+2\chi(1-\bar{\phi}_s)\right]}{1+\alpha_f} + \frac{\mathcal{G}\bar{\phi}_s}{1+\alpha_f}\left[1+\left(\frac{1+\alpha_f}{1-\bar{\phi}_s}\right)^2\right]. \tag{43}$$

Note here, that for $\alpha_f = O(\xi) = r\xi$, with $r > 0$ the stability analysis still holds with a factor

$$a_{++}^{(-1)} \sim \frac{2 + r\bar{\phi}_n^{(0)}}{1 + r\bar{\phi}_n^{(0)}}\frac{1}{\xi}, \tag{44}$$

which leads to the same condition for $a_{ss}^{(0)}$, whose leading order term is the same as in the previous section given $\alpha_f = 0$. Also note, that when setting $\alpha_f = 0$ we retrieve the exact same condition as for phase separation in hydrogels [13]. It is now apparent that the presence of fixed charges enhance the stability of the system. As shown in Figure 4, the region of instability shrinks.

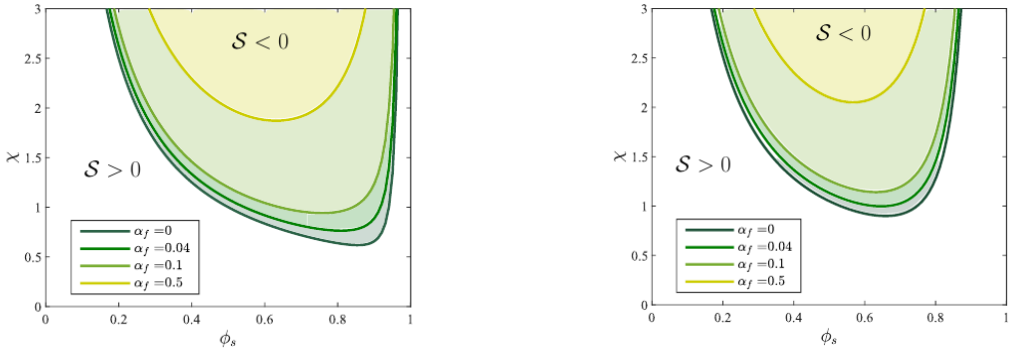

(a) $\mathcal{G} = 0.0002$ **(b)** $\mathcal{G} = 0.01$

Figure 4: Effect of the fixed charges on the stability region of an homogenous steady state. The latter is unstable in the region above the curve, we thus conclude that the presence of fixed charges tends to stabilize the system at least at leading order in the dilute case.

	α_f	$\mathcal{D}_+$	$\mathcal{D}_-$	χ	$\mathcal{G}$	ω	θ	c_0^-	c_0^+
1	0.04	5	5	0.78	0.0002	0.025	0	5×10^{-6}	0.0001
2	0.04	5	5	0.78	0.0002	0.025	0	5×10^{-6}	0.01

Table 1: Values of the parameter used in the simulation. The last two columns represent the salt concentration in the bath before the start of the simulation at $t = 0$ and the latter the value to which it is raised to after that. This drives the deswelling of the gel for $t > 0$.

Nonlinear evolution of an unstable homogeneous gel

In this section, we investigate how the instability develops from a slightly perturbed homogeneous gel and evolves beyond the region of validity of the linear stability analysis. For this purpose, we solve the system (10), (11), (12) and (13) numerically, first mapping z to a fixed domain via $Z = z/h(t)$, then discretising the result using a finite difference method on a staggered-grid. The fluxes are evaluated on the edges while volume fractions and chemical potentials on the cell midpoints. For the time-evolution we have used a semi-implicit method that treats linear term implicitly while approximate non-linear term explicitly [13].

For the initial conditions, we let the system equilibrate with the bath for a combination of parameters for which a simple change in χ will take us into the unstable regime. In this case, we start with $\chi = 0.78$, with the other parameters given in the caption of Fig. 5. The equilibrium is then given by the red line in the rightmost panel of the figure. The equilibrium state $\bar{\boldsymbol{\phi}} = (\bar{\phi}_s, \bar{\phi}_+, \bar{\phi}_-)$ is implicitly defined by the following system of three algebraic equation:

$$\boldsymbol{F}_{eq}(\chi, c_0, \bar{\boldsymbol{\phi}}) = \begin{bmatrix} F_s(\bar{\phi}_s, \bar{\phi}_+, \bar{\phi}_-; \chi, \mathcal{G}) - \ln(1 - 2c_0) \\ F_+(\bar{\phi}_s, \bar{\phi}_+, \bar{\phi}_-; \chi, \mathcal{G}) - \ln(c_0) \\ F_-(\bar{\phi}_s, \bar{\phi}_+, \bar{\phi}_-; \chi, \mathcal{G}) - \ln(c_0) \end{bmatrix} = \mathbf{0}, \tag{45}$$

where we impose the continuity of the chemical potential in the gel and the bath. Considering the elasticity of the gel $\mathcal{G}$ to be fixed, we investigate how the equilibrium curve depends on the concentration of ions in the bath c_0 and the enthalpy parameter χ, which is related to the temperature at which the experiment is conducted. As shown in Figure 2a, for small $\mathcal{G}$, the system undergoes a bifurcation. As we change the control parameter χ and c_0, we can move from a regime with three equilibrium states $\bar{\boldsymbol{\phi}}(\chi, c_0)$ to a single one. As illustrate in Figure 2b, modulating the concentration of oxygen in the bath, we will able to induce the development of depletion front that connects an highly swollen state (at $t = 0$) to a collapsed one. As previously discussed in [4], by increasing the shear modulus $\mathcal{G}$ (as for Figure 5), we have no remarkable change in the behaviour of the system (i.e. there is a unique steady state).

Then, we increase χ to $\chi = 1.2$, which is in the unstable regime as depicted in Fig. 5. To provide some noise, we let a small amount of liquid drain from the gel before we remove the gel from the bath and impose a no-flux boundary condition at $z = h(t)$. Instantly, rapidly growing perturbations set in that rapidly fill the entire length of the gel and then begin to coarsen or collide, resulting in fewer and broader spikes. Over time, the evolution slows down until the pattern is almost stationary. However, we expect that in principle coarsening continues until only two regions remain, one in the dry state at about $\phi = 0.3$ and the other just below 1. These two end state values are stable as indicated in the rightmost panel in the figure.

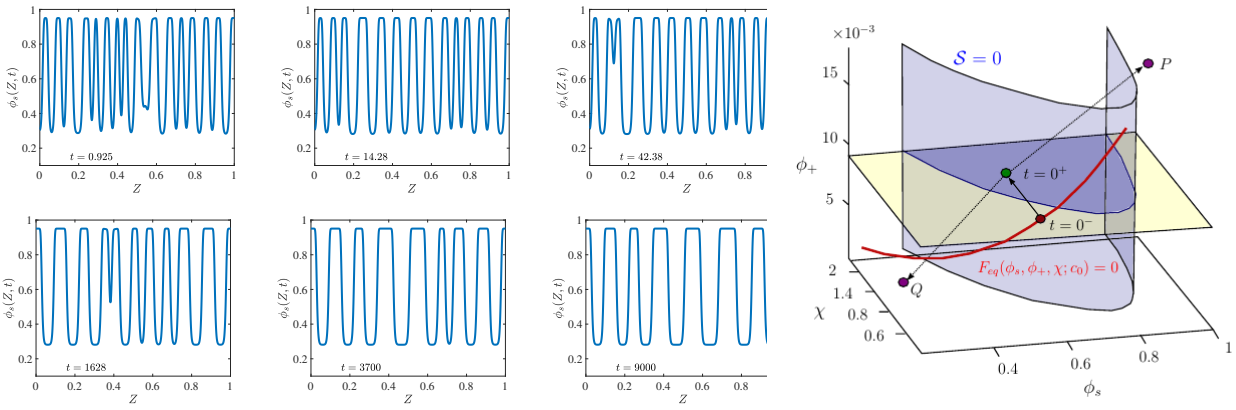

Figure 5: Evolution of the solvent fraction ϕ_s for the electro-neutral limit. The gel is initially at equilibrium with the bath $c_0 = 5 \times 10^{-3}$. The initial condition is a noisy state around the homogeneous equilibrium for $\chi = 0.78$ (see phase plane). Simulation are run for $\mathcal{G} = 0.001$, $\chi = 1.2$, $\omega = 0.01$, $\alpha_f = 0.04$ and $\mathcal{D}_+ = \mathcal{D}_- = 5$. As shown in the phase plane, by increasing χ we move into the region of the plane where the system is unstable, so that the perturbations grow giving rise to a sequence of spikes, which slowly merge. The red curve indicates the equilibrium curve in the 3D space. The yellow plane identifies $\phi_+ = \phi_+(0)$ which is equal to the equilibrium fraction of positive charge for $\chi = 0.78$. At time $t = 0^+$ by changing χ we move into the unstable region which drives the formation of the spikes. The point P and Q represent the peak and the trough of the spikes, that we can see lie in the stable region of the phase plane.

4 Collapse of a gel

The intriguing property of a polyelectrolyte gel in a salt solution is that not only swelling but the collapse of a gel is very sensitively dependent on small variations of the salt (c_0) concentration. We now study numerical results from the first set (set 1) of parameters in Table 1. As before, we discretise the system of equation using a finite difference method on a staggered-grid. This time however, given the different boundary condition, fluxes are evaluated on the cell midpoints while volume fractions and chemical potentials on the cell edges. Again the we have used a semi-implicit method that treats linear term implicitly while approximate non-linear term explicitly [13]. Note however that in this case also the boundary conditions (13) are non linear. Since we are interested in accurately capturing the interplay between the bath and the gel, we use fixed point iterations. More details can be found in Appendix. For the initial condition, the gel is equilibrated with a bath with a small salt concentration c_0^-. At $t = 0$, it is then placed into a solution with a higher salt concentration c_0^+. On an order one time scale, the mobile ion concentrations, adjust through to their new values. This is shown in Fig. 6 for c_0^+. Within less than one time unit, the concentration builds up at the boundary and penetrates into the gel. At $t = 12$, the process has almost concluded and in fact, early signs of a new wave manifest themselves at the free interface, which becomes more pronounced at $t = 301$. Together with the mobile ion concentration, the chemical potentials $\mu_\pm$ move from their initial value $\ln(c_0^-)$ to approximately $\ln(c_0^+)$. This difference in chemical potential drives the process of ion diffusion. Since the flux of ions is $D_\pm$ times the gradient of the chemical potential (with a domain of size 8), we obtain that $\mathcal{O}(1)$ changes of $\phi_\pm$ occur on an $\mathcal{O}(1)$ time scale, consistent with the observation in the numerical simulations.

After the mobile ion concentration has adjusted, a slower process takes place, whereby solvent is removed from the gel through the aforementioned wave, or depletion front. The front is clearly seen in the concentration profiles for the solvent ϕ_s as well as for the mobile ion species $\phi_\pm$ and the electrical potentials. The position of the front is shown for three different times in Fig. 7. In the last column, the wave has reached the substrate and the gel has collapsed and its composition settles into a new state. The main contribution to the solvent transport comes from gradients of μ_s, which here is small, only on the order of 10^{-4}, and a diffusion constant that has been scaled to 1. Hence the appropriate time scale for the depletion front movement is 10^4. This value of μ_s is set by F_s, and is connected with $\mathcal{G}$, which is small and this therefore determines the slow collapse.

The evolution of the gel can be summarised in Fig. 1(b) and (c), which depicts the state of the gel at a fixed position $Z = 0.4$. In the beginning, the gel has a high concentration of solvent and a low one in the ϕ_+. It quickly changes to a new state with higher salt content. Both of these states are stable and show no sign of spinodal decomposition. Instead, a depletion front moves through, first raising the solvent concentration slightly to the value at time point C and then decreasing it to D, with a similar salt but a much lower solvent concentration. All of these states lie in the linearly stable parameter regime.

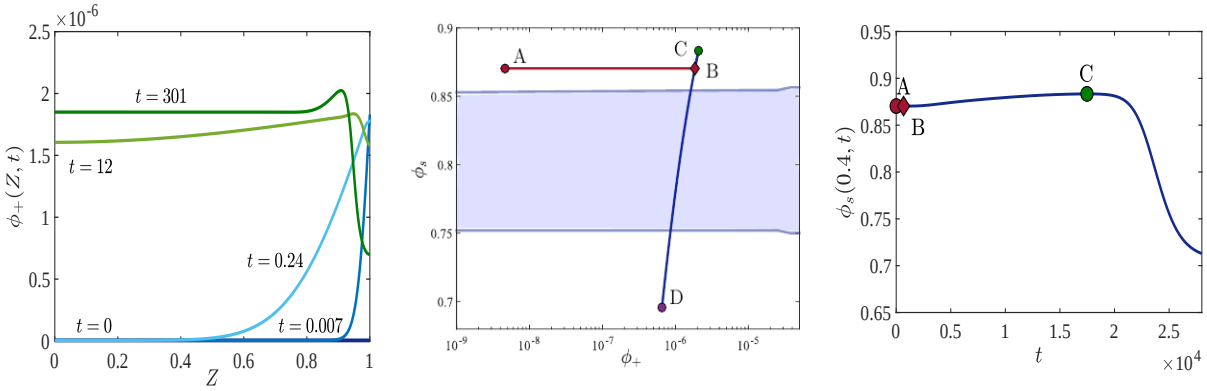

Figure 6: Results for the parameter set 1, from left to right: (a) evolution of the ion fraction $\phi_+(Z,t)$ in the gel at order one times; (b) evolution of the solution in the (ϕ_s, ϕ_+) plane: the instability region as predicted by the stability analysis for the electro-neutral limit is highlighted in blue; (c) evolution of the solvent fraction ϕ_s at location $Z = 0.4$ over time.

4.1 Phase-plane analysis

Assume $\partial_t\phi_s$, $\partial_t\phi_\pm$, $\partial_t(\phi_s v_n^2)$, j_s^2, $\partial_t(\phi_\pm v_n^2)$, $j_\pm^2 \ll 1$. Then we can conclude from (11a), (11b) that $\mu_s, \mu_+\, \mu_-$ are constant (independent of z), so that we have

$$\mu_s = \mathcal{G}p - \omega^2\partial_{zz}\phi_s + \ln\phi_s + [\chi(1-\phi_s)+1]\phi_n \tag{46a}$$
$$\mu_\pm = \mathcal{G}p \pm \Phi + \ln(\phi_\pm) + (1-\chi\phi_s)\phi_n \tag{46b}$$
$$-\beta^2\partial_{zz}\Phi = \phi_+ - \phi_- + \alpha_f\phi_n \tag{46c}$$
$$p = \frac{\omega^2}{\mathcal{G}}\left[\phi_s\partial_{zz}\phi_s - \frac{1}{2}(\partial_z\phi_s)^2\right] + \frac{\beta^2}{2\mathcal{G}}(\partial_z\Phi)^2 + \frac{1-\phi_n^2}{\phi_n}, \tag{46d}$$
$$\phi_n + \phi_s + \phi_- + \phi_+ = 1. \tag{46e}$$

Here we have specialised to the case $z_+ = 1$ and $z_- = -1$.

We will only consider the case $\beta \ll \omega \ll 1$. After first rescaling the system by $z = \omega\tilde{z}$, and then dropping the tilde, we obtain, to leading order in β/ω,

$$\mu_s = \mathcal{G}p - 2\partial_{zz}\phi_s + \ln\phi_s + [\chi(1-\phi_s)+1]\phi_n, \tag{47a}$$
$$\mu_\pm = \mathcal{G}p \pm \Phi + \ln(\phi_\pm) + (1-\chi\phi_s)\phi_n, \tag{47b}$$
$$0 = \phi_+ - \phi_- + \alpha_f\phi_n, \tag{47c}$$
$$p = \frac{1}{\mathcal{G}}\left[\phi_s\partial_{zz}\phi_s - \frac{1}{2}(\partial_z\phi_s)^2\right] + \frac{\beta^2}{2\mathcal{G}}(\partial_z\Phi)^2 + \frac{1-\phi_n^2}{\phi_n}, \tag{47d}$$
$$\phi_n + \phi_s + \phi_- + \phi_+ = 1. \tag{47e}$$

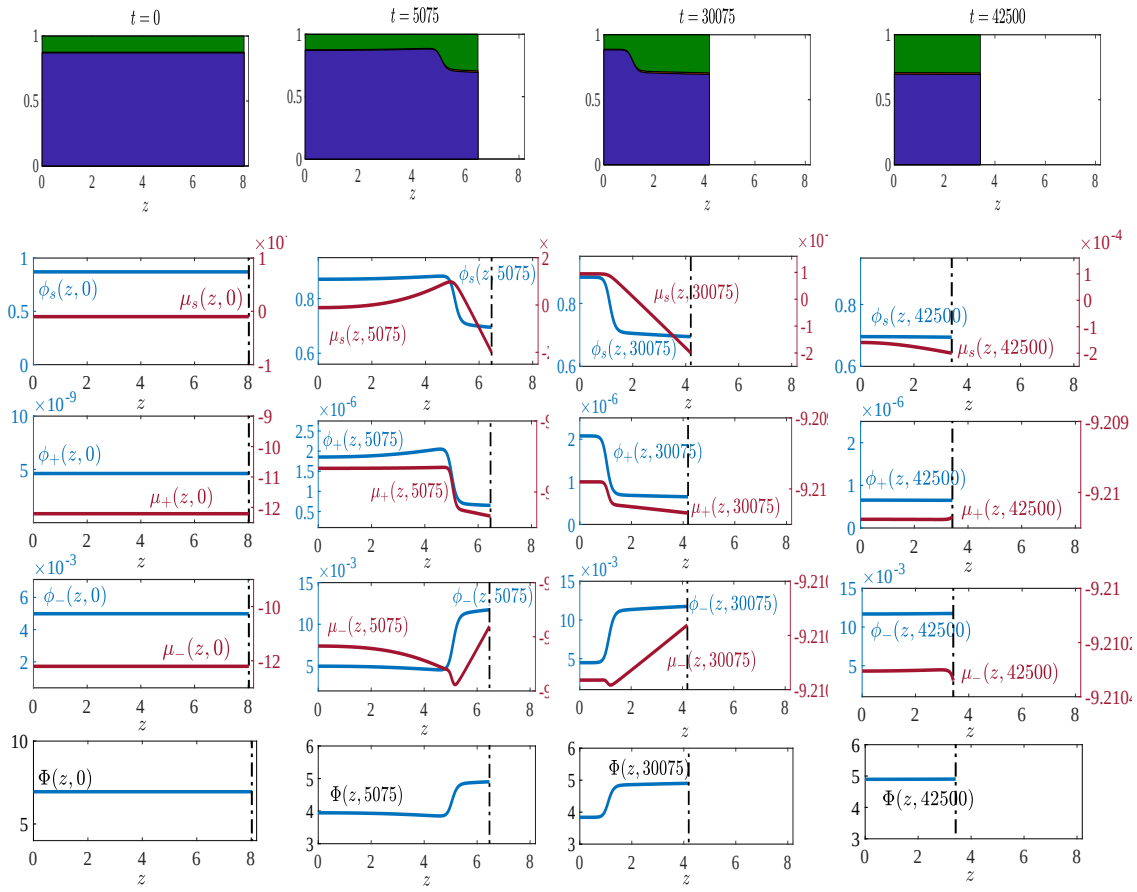

Figure 7: Gel composition and state variables at different times for parameter set 1.

This can be condensed to the form

$$\partial_z \phi = q \tag{48a}$$

$$\partial_z q = \frac{1}{1-\phi}\left[B(\phi,n) - \mu_s\right] - \frac{1}{2(1-\phi)}q^2 \tag{48b}$$

$$\mu_s = \frac{\phi - 1}{\phi}\left[\frac{\mu_+ + \mu_-}{2} - A(\phi,n)\right] + B(\phi,n) - \frac{1}{2\phi}q^2, \tag{48c}$$

with

$$A(\phi,n) = \frac{1}{2}\ln\left[\frac{1}{4}\left(n^2 - \alpha_f^2(1-\phi-n)^2\right)\right] + (1-\chi\phi)(1-\phi-n) + \mathcal{G}\frac{1-(1-\phi-n)^2}{1-\phi-n}, \tag{48d}$$

$$B(\phi,n) = \ln(\phi) + (\chi(1-\phi)+1)(1-\phi-n) + \mathcal{G}\frac{1-(1-\phi-n)^2}{1-\phi-n}, \tag{48e}$$

where $\phi \equiv \phi_s$ and $n \equiv \phi_+ + \phi_-$, and where we have also introduced the auxiliary variable q. Instead of n, it is often useful to formulate the system using ϕ_+ as the dependent variable, which can be easily done by using the electro-neutrality condition (47c) and (47e), so that

$$n = \frac{\alpha_f}{1+\alpha_f}(1-\phi) + \frac{2}{1+\alpha_f}\phi_+. \tag{49}$$

Equilibria (flat states) are found from (48) via

$$A(\phi, n) = \frac{\mu_+ + \mu_-}{2}, \quad B(\phi, n) = \mu_s. \tag{50}$$

The limit of dilute salt concentrations

We wish to obtain solutions connecting two different equilibria emerging from (50), and we will first do so for the case of sufficiently small salt concentrations. We note that from the electro-neutrality condition (47c), it is clear that ϕ_- and $\alpha_f \phi_n$ have to balance, suggesting that ϕ_- and n scale like α_f. From the observation we made in (18), we have that ϕ_+ should scale like $(c_0^+)^2/\alpha_f$. Thus $(1/2)\ln(\phi_+\phi_-) \sim \ln(c_0^+)$. This is a large term (for small c_0) which has to be balanced with another term in A if the first equation of (50) is to be satisfied. The only candidate for this is $(\mu_+ + \mu_-)/2$, which therefore has to have $\mathcal{O}(\ln(c_0^+))$, This is consistent with the numerical results e.g. in Fig. **??**, where we see that $\mu_\pm = -9.21 \approx \ln(c_0^+)$.

These estimates suggest introducing the new variables

$$n = \alpha_f \tilde{n}, \quad \phi_- = \alpha_f \tilde{\phi}_-, \quad \phi_+ = ((c_0^+)^2/\alpha_f)\tilde{\phi}_+, \quad \mu_\pm = \ln(c_0) + \tilde{\mu}_\pm, \tag{51}$$

hence

$$\tilde{n} = \frac{1}{1+\alpha_f}\left(1 - \phi + 2\gamma^2 \tilde{\phi}_+\right). \tag{52}$$

Here, we have introduced another dimensionless parameter

$$\gamma = \frac{c_0^+}{\alpha_f}. \tag{53}$$

We note that it can be seen from the numerical data that $\tilde{\mu}_\pm$ is small; on the order of $10^{-4}\ln(\gamma\alpha_f)$.

For the values in Table 1, we have that $\gamma \ll 1$; hence we first consider the leading order problem in this limit. We obtain

$$\partial_z \phi = q \tag{54a}$$

$$\partial_z q = \frac{1}{1-\phi}\left[B_0(\phi) - \mu_s\right] - \frac{1}{2(1-\phi)} q^2 \tag{54b}$$

$$\tilde{\mu}_s = \frac{1-\phi}{\phi}\left[A_0(\phi, \tilde{\phi}_+) - \frac{\tilde{\mu}_+ + \tilde{\mu}_-}{2}\right] + B_0(\phi) - \frac{1}{2\phi} q^2, \tag{54c}$$

with

$$A_0(\phi, \tilde{\phi}_+) = \frac{1}{2}\ln\left[\left(\frac{1-\phi}{1+\alpha_f}\right)\tilde{\phi}_+\right] + (1-\chi\phi)\left(\frac{1-\phi}{1+\alpha_f}\right) + \mathcal{G}\frac{(1+\alpha_f)^2 - (1-\phi)^2}{(1+\alpha_f)(1-\phi)}, \tag{54d}$$

$$B_0(\phi) = \ln(\phi) + (\chi(1-\phi)+1)\left(\frac{1-\phi}{1+\alpha_f}\right) + \mathcal{G}\frac{(1+\alpha_f)^2 - (1-\phi)^2}{(1+\alpha_f)(1-\phi)}. \tag{54e}$$

The two ODEs (54a) and (54b) decouple from the algebraic constraint (54c). Combining these into a second order equation and obtaining an integrating factor $f = 1/\sqrt{1-\phi}$ results in

$$\frac{(\partial_z \phi)^2}{2(1-\phi)} = \int_{\phi_1}^{\phi} \frac{B_0(\eta) - \mu_s}{(1-\eta)^2} \mathrm{d}\eta. \tag{55}$$

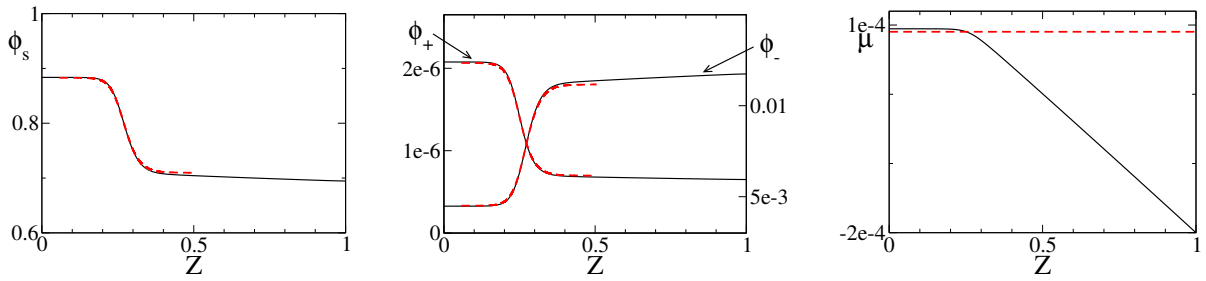

Figure 8: Comparison of the asymptotic approximation for the phase plane solution (54), (56), (57) (shown with dashed red lines) for (a) $\phi = \phi_s$ and (b) ϕ_+ together with ϕ_- and (c) $\mu = \mu_s$ with the numerical results from Fig. **??** (solid black lines), using the parameter set 1 in Table 1. A single shift along the z-axis was applied to all phase plane profiles so that ϕ_s matches the numerical solution at $\phi = 0.8$. In (b), each of the symbols ϕ_+ and ϕ_- is displayed on the axis with the corresponding values.

Letting $z \to +\infty$ gives the condition

$$\int_{\phi_1}^{\phi_2} \frac{B_0(\phi) - \mu_s}{(1-\phi)^2} \mathrm{d}\phi = 0, \tag{56}$$

which, together with

$$B_0(\phi_1) - \mu_s = 0, \quad B_0(\phi_2) - \mu_s = 0, \tag{57}$$

results in a nonlinear system of equations for ϕ_1, ϕ_2 and μ_s. Solving the equation with the parameters for α and χ and g corresponding to Fig. **??** (i.e. parameter set 1 in Table 1) gives

$$\mu_s = 0.903 \times 10^{-4}, \quad \phi_1 = 0.883, \quad \phi_2 = 0.710. \tag{58}$$

Once ϕ is determined, ϕ_+ and ϕ_- can be recovered from (54c) and from

$$\phi_- = \frac{\alpha_f}{1+\alpha_f}(1-\phi) - \frac{1-\alpha_f}{1+\alpha_f}\phi_+, \tag{59}$$

provided $(\tilde{\mu}_+ + \tilde{\mu}_-)/2$ is known from the numerical simulations. For $\tilde{\phi}_{+,1}$ and $\tilde{\phi}_{+,2}$, i.e. the values at the left and right flat state of the depletion front, we obtain

$$\tilde{\phi}_{+,1} = 8.25, \quad \tilde{\phi}_{+,2} = 2.79. \tag{60}$$

In Fig. 8(a) and (b), we compare the profiles for ϕ, ϕ_+ and ϕ_- obtained in this way. For the latter two, we need to specify $(\tilde{\mu}_+ + \tilde{\mu}_-)/2$, which is not selected by the asymptotic result at this level of approximation. The results shown in the figure were obtained by setting $(\tilde{\mu}_+ + \tilde{\mu}_-)/2$ to zero, while the numerical simulations suggest a value with absolute value of about 2×10^{-4}. Using this value instead did not visibly change the results on the scale of the graphs. A comparison of the constant asymptotic value $\mu = \mu_s$ from (58) with the result from the numerical simulation is also shown, in Fig. 8(c). There is very good agreement of the constant asymptotic value with the flat part of the graph from the simulations.

The general case

Returning to the full problem (48), we linearise around the equilibria to determine the number of modes consistent with the boundary conditions at $z \to \pm\infty$ and carry out a degree of freedom count. We make the ansatz

$$\phi = \bar{\phi} + \delta\phi_1 \mathrm{e}^{sz}, \quad q = \delta q_1 \mathrm{e}^{sz}, \quad n = \bar{n} + \delta n_1 \mathrm{e}^{sz}, \tag{61}$$

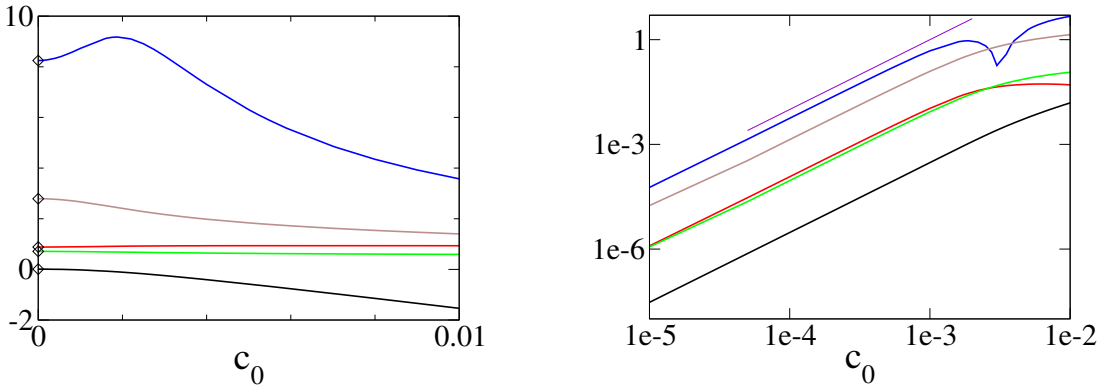

Figure 9: (a) The figure shows graphs of 100μ, ϕ_1, ϕ_2, $\tilde{\phi}_{+,1}$ and $\phi_{+,2}$, listed in order from bottom to top. The diamonds at $c_0 = 0$ represent the values obtained from the asymptotic solution as given by (58) and (60). We remark that μ is positive for $c_0 \leq 5.45 \times 10^{-3}$, and negative for larger values of c_0. (b) This log-log plot has graphs for $|\mu - \mu^{(0)}|$, $\phi_1 - \phi_1^{(0)}$, $\phi_2 - \phi_2^{(0)}$, $\tilde{\phi}_{1,+} - \tilde{\phi}_{1,+}^{(0)}$, $|\tilde{\phi}_{2,+} - \tilde{\phi}_{2,+}^{(0)}|$, where the superscript (0) indicates the asymptotic values from (58) and (60). The short top line represents a quadratic function, and is included to guide the eye.

with $\delta \ll 1$ and some constant s, and where $(\bar{\phi}, \bar{n})$ represents any pair of equilibrium that satisfy (50). Inserting this, we obtain from first order in δ the condition

$$\begin{bmatrix} B_\phi(\bar{\phi},\bar{n}) - (1-\bar{\phi})s^2 & B_n(\bar{\phi},\bar{n}) \\ (1-\bar{\phi})A_\phi(\bar{\phi},\bar{n}) + \bar{\phi}B_\phi(\bar{\phi},\bar{n}) & (1-\bar{\phi})A_n(\bar{\phi},\bar{n}) + \bar{\phi}B_n(\bar{\phi},\bar{n}) \end{bmatrix} \begin{bmatrix} \phi_1 \\ n_1 \end{bmatrix} = 0 \tag{62}$$

on s and ϕ_1, n_1. Here, the subscripts ϕ and n denote derivatives with respect to these variables. Setting the determinant of the coefficient matrix to zero gives

$$s^2 = \frac{A_n B_\phi - A_\phi B_n}{(1-\bar{\phi})A_n + \bar{\phi}B_n}. \tag{63}$$

In the limit $\gamma \to 0$, the derivatives A_n, A_ϕ and B_ϕ are $\mathcal{O}(1)$ but $B_n \to 0$, hence, $s^2 \sim B_\phi/(1-\bar{\phi})$. Also we recover the value μ_s and the two values ϕ_1 and ϕ_2 obtained from (56), (57). These are only two of the equilibria, but in fact the two which have $B_\phi > 0$. Hence, for small γ, we have $s^2 > 0$ and there is exactly one decaying and one growing mode on either side, $z \to -\infty$ and $z \to +\infty$. The decaying mode in each of these limits contributes one degree of freedom, μ_s and $\mu_+ + \mu_-$ another one each. The ODE systems is second order and hence removes two degrees of freedom, and the translational invariance of any solution towards shifts along the z-axis another one. Hence one degree of freedom remains, and this is consistent with our previous observation that there is one free parameter left, namely, $\mu_+ + \mu_-$. For larger values of γ, the sign of (63) could change, leading to purely imaginary s. This would manifest itself in the form spiral in phase space near the equilibrium, and hence a decaying spatial oscillation in the solution, but this was not observed for the depletion solutions documented in this article. Hence all of these are characterised by $s^2 > 0$ and follow the degree of freedom count just explained.

The general case of (48) was solved by shooting, using slightly perturbed values for the left state and integrating the resulting initial value problem for a system of differential algebraic equations (DAEs), rewritten in terms of ϕ and ϕ_+ as the dependent variables using Matlab's ode15i routine. Except where otherwise stated, we set $\mu_- + \mu_+ = 0$. For analytical solution, the trajectory would connect to the right equilibrium only for the correct values of μ_s, so we have to iterate over these. At or close to such μ_s, the trajectory connects to right flat state but the numerical solution always eventually departs and either hits zero in a singularity or moves back and forth between the two flat states. The different behaviour coincides with μ_s either being larger or lower than the correct value and hence it was used for a bisection iteration. The resulting solution defines μ_s and the associated values for the left and right state ϕ_1 and ϕ_2 for ϕ and similarly for the equilibrium values of the other variables ϕ_+ and ϕ_-.

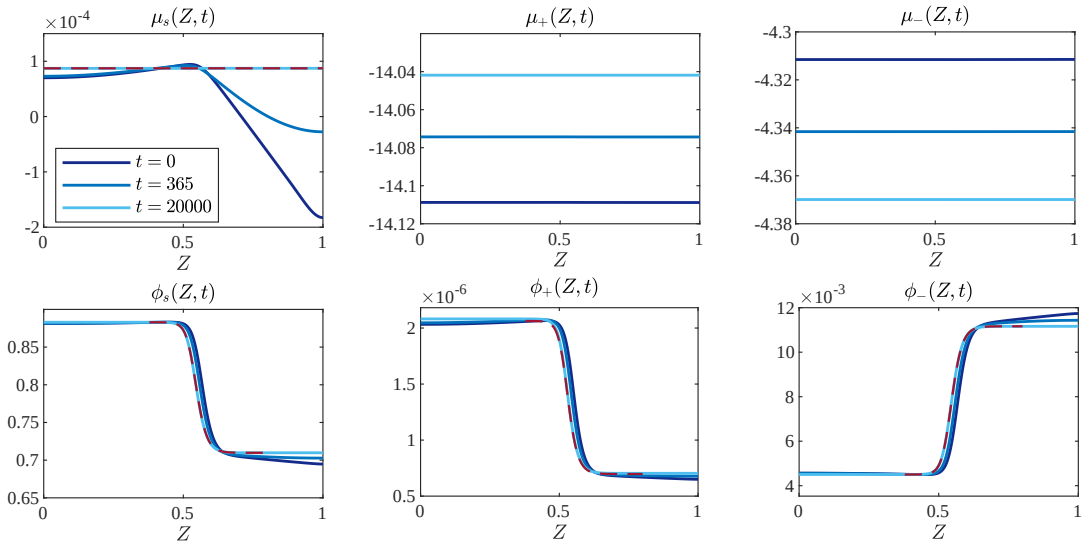

Figure 10: Spatial distribution of the variables at different times. We start with the results from the simulations for parameter set 1 in Figure 7 at time $t = 15075$. This provides the initial conditions for the results shown here. The gel is taken out of the bath and isolated so that the solvent is trapped in the gel. The system relaxes towards a non-homogeneous steady state where the depletion front - now a stationary phase boundary - divides the highly and poorly swollen region of the gel. The red line is the prediction from the phase space analysis.

The results are shown in Fig. 9. The plots in (a) show graphs of the values for 100μ and for the values of the two equilibrium states for ϕ and ϕ_+ as a function of the salt concentration c_0. For $c_0 \to 0$, the solution converges to the values given by the leading order asymptotic solution given by (56) and (57). Moreover, near to $c_0 = 0$, the behaviour is quadratic, as can be seen from the log-log plot in Fig. 9 (b), consistent with neglecting and $\mathcal{O}(\gamma^2)$ term in (54). However, for c_0 above about 1×10^{-3}, the value for $\tilde{\phi}_{+,2}$ departs from this behaviour and in fact passes through a maximum as it reverses its trend.

For a closer comparison of the simulation with solutions from the system of DAEs, we consider a situation where the influx of salt and solvent is stopped by removing the gel from the bath, after the depletion front has moved deep into the gel. As a result, the variables settle into a stationary state. The evolution and the final states are shown in Fig. 10, for the set 1 in Table 1. The fluxes become zero and the chemical potentials μ_S, μ_+ and μ_- become spatially homogeneous. The profiles for $\phi = \phi_S$, ϕ_+ and ϕ_- become exact stationary fronts, as in particular the dry gel portion takes on a single value (rather than showing a small gradient between the bath and the depletion front). Comparing these results with the solutions from the DAE are almost perfect, which are shown in Fig. 10 as thin red lines. Also, the results for $\mu_s = 2.45 \times 10^{-2}$ agree to within less than 1% of this value. To solve (48), we need to specify a value for $\mu_+ + \mu_-$ (or more specifically, for the difference $\tilde{\mu}_+ + \tilde{\mu}_-$ from $\ln(c_0)$). This turned out to be too large to simply it to zero, we instead read it off from the numerical solution, which gave us a nearly constant value $\tilde{\mu}_+ + \tilde{\mu}_- = 11.2 \times 10^{-2}$.

4.2 Spinodal decomposition of a collapsing gel

In this section we show that spinodal decomposition and the formation of a depletion front are independent phenomena which can also occur at the same time. An example of this is shown in Fig. 11, which are numerical simulation results for set 2 in Table 1. The only difference between set 1 and set 2 is the concentration c_+ in the bath. The higher concentration for the second set lies in the unstable parameter regime, see Fig. 11, so that, as soon as the mobile ions have diffused into the gel, the instability sets in. This gives rise to a series of spike depletions (“upside down” spikes), which coarsen/collide first rapidly and then very slowly. On a longer time scale, a depletion front develops and moves into

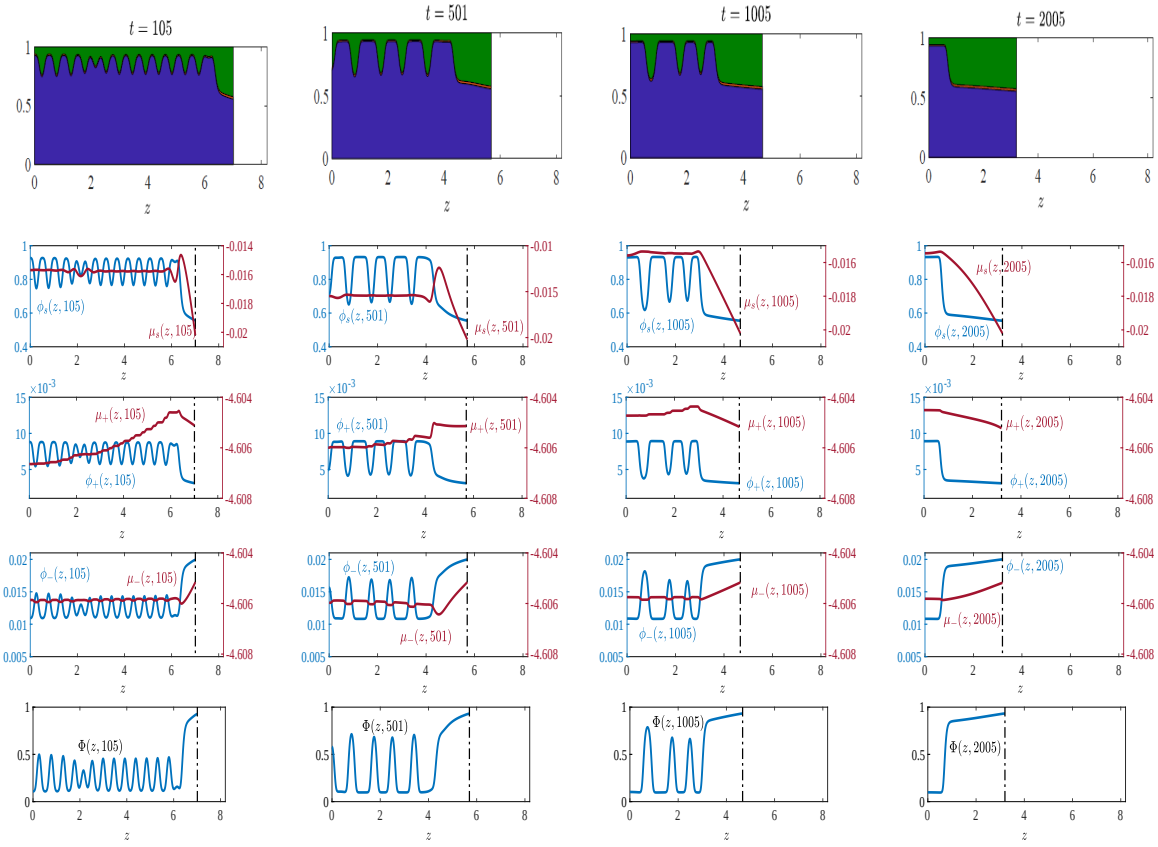

Figure 11: Gel composition and state variables at different time points for parameter set 3.

the gel, slowly consuming the array of holes. A comparison with depletion fronts obtained from the full model via phase space analysis shows that while there is some agreement, the slope is slightly too shallow and the lower limit of the front does not capture the right state of the front very well. In fact, the comparison with the side walls of a typical front is much better. A possible explanation of the higher discrepancy in the former case is that the holes evolve more slowly than the incoming wave.

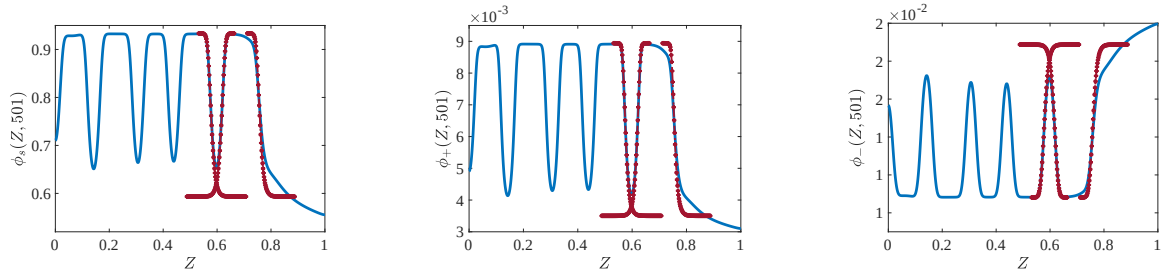

Figure 12: Comparison of the phase plane solution for $\phi = \phi_S, \phi_+$ (shown with dashed red lines and symbols) and ϕ_- with the numerical results at time $T = 501$ in Fig. 11, using set 2 from Table 1.

5 Conclusions

In this study we have focussed on the stability of homogeneous states and the transient dynamics between equilibria for a new model for a polyelectrolyte gel in a bath of salt solution. The model accounts for the free energy of the internal interfaces that form upon phase separation of the gel, deliniating regions where the gel network is collapsed.

We discuss the stability of the system for different regimes that are characterized by the ratio of parameters β/ω, the Debye-length to the width of the interface between the swollen and collapsed phase of the gel, and $\gamma = c_0/\alpha_f$, the ratio of the salt concentration in the bath and of the fixed charges on the polymer network, for the electro-neutral limit $\beta/\omega \ll 1$, and the dilute limit $\gamma \ll 1$, in the one-dimensional setting. We use numerical simulations to show that the unstable homogeneous solutions spinodally decomposed forming localized collapsed dry regions with high concentrations of ϕ_- ions, that eventually coarsen into a new stable equilibrium. We found that typically spinodal decomposition begins at the free interface with the salt solution, where the collapse of the gel is shown to arise from a depletion front that forms via phase separation and travels into the gel. Our phase-plane analysis shows that the depletion front selects the homogeneous states in front and behind of it and these

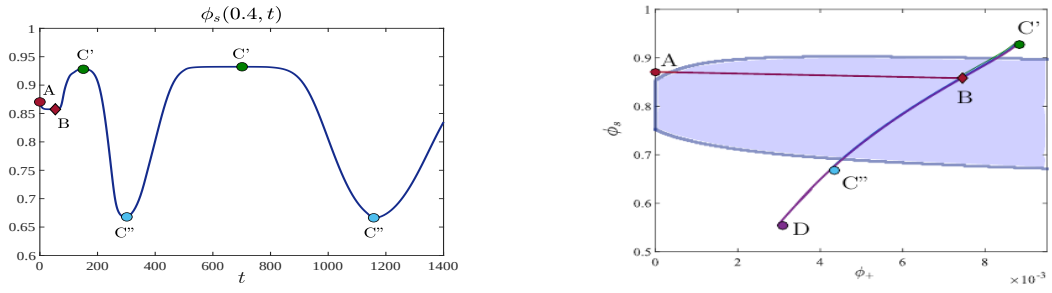

(a) $\phi_s(0.4,t)$ **(b)**

Figure 13: (a) Evolution of the solvent fraction ϕ_s at the position $Z = 0.4$ for set 2; (b) evolution of the solution in the (ϕ_s, ϕ_+) plane; the instability region as predicted by the stability analysis for the electro-neutral limit is highlighted in blue. (c) Map of the unstable parameter regimes for the set 1.

are always linearly stable. Also in the spinodal unstable case, the emerging localized dry regions are merged with depletion front that propagates through the gel. Evene though our analysis is currently only one-dimensional, it should be interesting to observe these patterns in an experiment. Depending on parameter settings, the periodic high concentration of ϕ_- in the dry and high concentration of ϕ_+ in swollen regions could be observed as a transient, coarsening pattern.

Further extensions of our model that accounts for concentration-dependent permittivity may allow to capture further collapse phenomena, observed for weakly-charged polyelectrolyte gels, will be carried our in upcoming work, as well as in higher dimensional formulations.

A The dilute sublimit $\phi_+ \ll 1$ for moderate to large β/ω

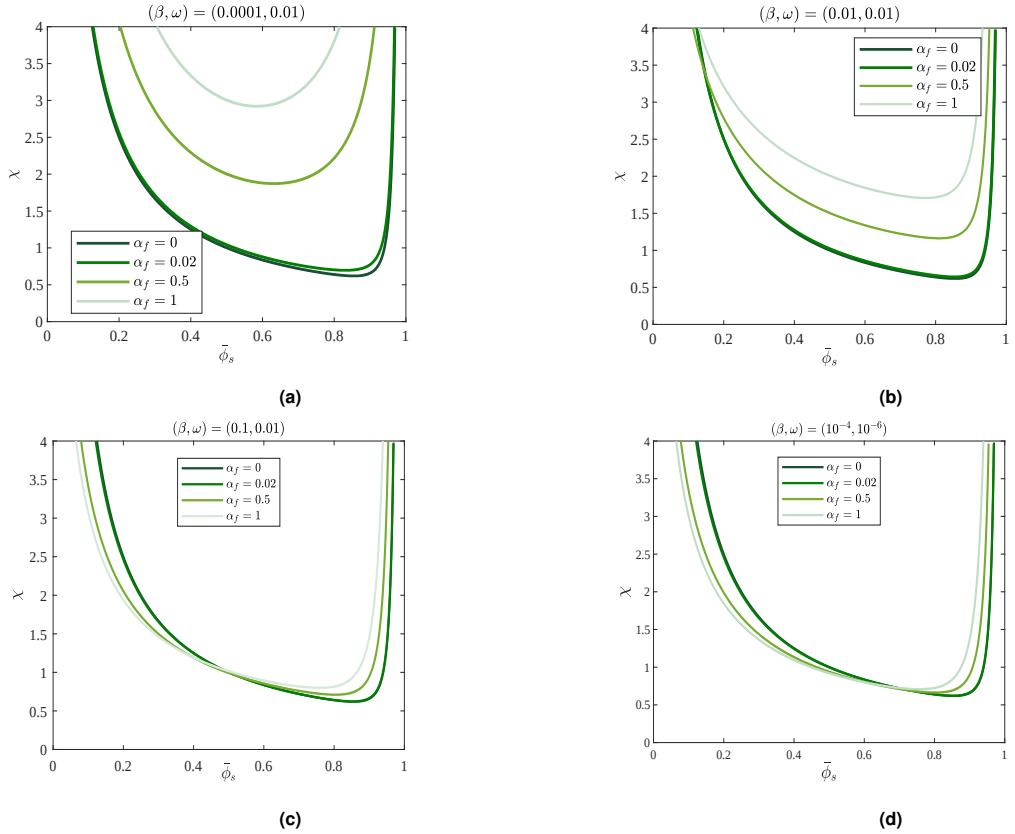

Figure 14: Effect of the size of the Debye Layer on the stability of the system. In the electro-neutral limit (a) we recover the result from Figure 4 where the fixed charges tend to stabilise the system. However, as we β becomes greater than ω the role of the fixed charges changes and drives the formation of instabilities in a 'collapsed' regime, where $\bar{\phi}_s < \bar{\phi}_n$.

We now investigate another limit of the system, which corresponds to the dilute case applied to the full model without imposing the electro-neutral limit. In such condition, the leading order components for the equilibrium states is:

$$\bar{\phi}_-(\bar{\phi}_s) = \frac{\alpha_f(1-\bar{\phi}_s)}{1+\alpha_f}, \quad \bar{\phi}_n(\bar{\phi}_s) = \frac{1-\bar{\phi}_s}{1+\alpha_f}. \tag{64}$$

As in the previous case we need to recall that $\partial F_+/\partial\phi_+$ is of order $O(\xi^{-1})$ so that we can not simply substitute $\xi = 0$ in the system (22) to obtain the leading term. The resulting equation for the growing

rate λ is still a third order equation as (23), which is however more trackable:

$$\beta^2 k^2 \lambda^3 + k^2 \mathcal{D} \lambda^2 \alpha_2^{(0)} + k^4 \mathcal{D} \lambda \alpha_1^{(0)} + \mathcal{D}^2 \bar{\phi}_- \bar{\phi}_n^{\theta+1} \bar{\phi}_s k^6 \alpha_0^{(0)} = 0, \tag{65}$$

In order to have only negative eigenvalues, all of the coefficient must be positive for any value of k. The latter are of the following form:

$$\begin{aligned} \alpha_2^{(0)}(k) = k^4 \omega^2 \beta^2 \left(\bar{\phi}_s \bar{\phi}_- \mathcal{D} + \bar{\phi}_n^{\theta+2} \right) + k^2 \beta^2 \Big[\mathcal{D} + \bar{\phi}_n^{\theta+1} \left(a_{ss}^{(0)} \bar{\phi}_s + \bar{\phi}_- a_{s-}^{(0)} \right) \\ + \bar{\phi}_- \left(\bar{\phi}_n^{\theta+1} - \mathcal{D} \bar{\phi}_s \right) a_{-s}^{(0)} + \bar{\phi}_- \left(\mathcal{D}(1 - \bar{\phi}_-) + \frac{\bar{\phi}_n^{\theta+1} \bar{\phi}_-}{\bar{\phi}_s} \right) a_{--}^{(0)} \Big] \\ + \mathcal{D} \bar{\phi}_- + \frac{\alpha_f^2 \bar{\phi}_n^{\theta+2}}{\bar{\phi}_s}, \end{aligned} \tag{66a}$$

$$\begin{aligned} \alpha_1^{(0)}(k) = k^4 \beta^2 \omega^2 \bar{\phi}_s \left[\mathcal{D} \bar{\phi}_- \bar{\phi}_s + \bar{\phi}_n^{\theta+2} + \bar{\phi}_n^{\theta+1} \bar{\phi}_- \left((1 - \bar{\phi}_s) a_{--}^{(0)} + \bar{\phi}_s a_{s-}^{(0)} \right) \right] \\ + k^2 \beta^2 \Big[\bar{\phi}_n^{\theta+1} \left(\bar{\phi}_s a_{ss}^{(0)} + \bar{\phi}_- a_{s-}^{(0)} \right) + \bar{\phi}_s \bar{\phi}_- \left(a_{--}^{(0)} a_{ss}^{(0)} - a_{-s}^{(0)} a_{s-}^{(0)} \right) \\ + \bar{\phi}_- \left(\bar{\phi}_n^{\theta+1} - \mathcal{D} \bar{\phi}_s \right) a_{-s}^{(0)} + \bar{\phi}_- \left(\mathcal{D}(1 - \bar{\phi}_-) + \frac{\bar{\phi}_n^{\theta+1} \bar{\phi}_-}{\bar{\phi}_s} \right) a_{--}^{(0)} \Big] \\ + k^2 \omega^2 (1 + \alpha_f)^2 \bar{\phi}_- \bar{\phi}_s \bar{\phi}_n^{\theta+2} + \bar{\phi}_- \bar{\phi}_n^{\theta+1} \bar{\phi}_s \left[(1 + \alpha_f) a_{ss}^{(0)} - \alpha_f a_{s-}^{(0)} \right] \\ + \mathcal{D} \bar{\phi}_- + \frac{\alpha_f^2 \bar{\phi}_n^{\theta+2}}{\bar{\phi}_s} \end{aligned} \tag{66b}$$

$$\begin{aligned} \alpha_0^{(0)} = \beta^2 \omega^2 k^4 \left(a_{--}^{(0)} \left(1 - \bar{\phi}_s \right) + a_{s-}^{(0)} \bar{\phi}_s \right) + k^2 \Big[\beta^2 \left(a_{--}^{(0)} a_{ss}^{(0)} - a_{-s}^{(0)} a_{s-}^{(0)} \right) \\ + \omega^2 \bar{\phi}_n \left(1 + \alpha_f \right)^2 \Big] + \left[(1 + \alpha_f) a_{ss}^{(0)} - \alpha_f a_{s-}^{(0)} \right], \end{aligned} \tag{66c}$$

where the coefficient $a_{ij}^{(0)}$ are defined as

$$a_{ss}^{(0)} = \frac{\partial F_s}{\partial \phi_s} (\bar{\phi}_\phi)^{(0)} = \mathcal{G} \left(1 + (\bar{\phi}_n^{(0)})^{-2} \right) + \frac{1}{\bar{\phi}_s} - 1 - \chi (1 - \bar{\phi}_s) - \chi \bar{\phi}_n, \tag{67a}$$

$$a_{s-}^{(0)} = \frac{\partial F_s}{\partial \phi_-} (\bar{\phi}_\phi)^{(0)} = \mathcal{G} \left(1 + (\bar{\phi}_n^{(0)})^{-2} \right) - 1 - \chi (1 - \bar{\phi}_s), \tag{67b}$$

$$a_{-s}^{(0)} = \frac{\partial F_-}{\partial \phi_s} (\bar{\phi}_\phi)^{(0)} = \mathcal{G} \left(1 + (\bar{\phi}_n^{(0)})^{-2} \right) - 1 + \chi \bar{\phi}_s - \chi \bar{\phi}_n, \tag{67c}$$

$$a_{--}^{(0)} = \frac{\partial F_-}{\partial \phi_-} (\bar{\phi}_\phi)^{(0)} = \mathcal{G} \left(1 + (\bar{\phi}_n^{(0)})^{-2} \right) - 1 + \chi \bar{\phi}_s + \frac{1}{\bar{\phi}_-}. \tag{67d}$$

Note however that, unlike for the electro-neutral case the coefficients $a_0(k)$ and $a_1(k)$ are fourth order polynomials and can therefore allow for the presence of multiple minima. Let us rewrite them as

$$\alpha_i^{(0)}(k) = \ell_i^{(2)} k^4 + \ell_i^{(1)} k^2 + \ell_i^{(0)}, \tag{68}$$

then the minimum value of the function given by:

$$\min \alpha_i^{(0)}(k) = \ell_i^{(0)} - \frac{(\ell_i^{(1)})^2}{4 \ell_i^{(2)}} H \left(-\frac{\ell_i^{(1)}}{\ell_i^{(2)}} \right) > 0. \tag{69}$$

For the set of parameter considered, we have that the stability region is delimited by the curve $\min \alpha_0(k) > 0$, so that we can define $\mathcal{S}$ is of the form

$$\mathcal{S} = \min a_0(k). \tag{70}$$

Note that in the limit of $\beta \to 0$, we recover the results for the electro-neutral model. Again, the stability of the system is not affected by the value of the diffusion coefficient $\mathcal{D}$, so that we focus on investigating how the other parameters α_f, ω and β affect the results.

We note that as β becomes larger than ω the role of the fixed charges changes. In the electro-neutral limit the latter facilitate the stability of the system. As shown in Figure 14, the curve $\mathcal{S}$ is translated upwards as the α_f grows. Once we move towards a regime in which $\omega \sim \beta$, as in Figure 14(b), the effect of the fixed charges is reduced with the shrinking of the stability region being less significant. As β dominates ω, we see the curve $\mathcal{S}$ moving towards the left thus favouring the formation of instabilities in poorly swollen gels ($\bar{\phi}_s < \bar{\phi}_n$) while increasing the stability of highly swollen states.

B Numerical methods

For the numerical implementation the following formulation of the system it is convenient to resize the moving domain onto a fixed one using the following change of variables:

$$Z = \frac{z}{h(t)}, \quad \frac{dh}{dt} = v_n|_{h(t)}\,. \tag{71}$$

The problem can be further simplified eliminating the electric potential. This can be retrieved by solving the following decoupled ODE:

$$\partial_Z \Phi = \frac{\partial F_-}{\partial \phi_s}\partial_Z \phi_s + \frac{\partial F_-}{\partial \phi_+}\partial_Z \phi_+ + \frac{\omega^2 \phi_s}{h^2}\partial_{ZZZ}\phi_s + \frac{j_+ h}{\mathcal{D}_- \phi_-} - \frac{j_s h}{\mathcal{D}_- \phi_s}, \tag{72a}$$

$$\Phi = \sinh^{-1}\left[\frac{\alpha_f \phi_n}{2c_0}\exp\left(\mathcal{G}p + \phi_n\left(1 - \chi c_s\right)\right)\right], Z = 1. \tag{72b}$$

Consequently, we solve at each time point t_i for only four dependent variable $\boldsymbol{y} = (\phi_s, \phi_+, j_s, j_+)$. As mentioned in the main text, for the governing equation, we use a staggered grid and a semi-implicit method for the space and time discretisation respectively. For the governing equations the non-linear term are treated explicitly, so as to linearise the system. For the boundary conditions, which reduce to:

$$j_s = j_+ = 0, \quad Z = 0, \tag{73a}$$

$$\partial_Z \phi_s = 0, \quad Z = \{0, 1\}, \tag{73b}$$

$$\partial_{ZZ}\phi_s = \frac{h^2(t)}{\omega^2\left(1-\phi_s\right)}\left[\mathcal{G}\frac{1-\phi_n^2}{\phi_n} + \left(\chi(1-\phi_s)+1\right)\phi_n + \ln\frac{\phi_s}{1-2c_0}\right], \quad Z = 1, \tag{73c}$$

$$\phi_+ = c_0 \exp\left[-\Phi - \mathcal{G}p - \left(1 - \chi\phi_s\right)\phi_n\right], \quad Z = 1. \tag{73d}$$

The no-flux boundary conditions are strongly imposed, while the Neumann condition of ϕ_s is approximated using ghost point. Less trivial instead is the treatment of the non-linear terms in (73c)-(73d), which relies on fixed point iteration. Consider we are solving for the time $t = t_{i+1}$ and we have the solution $\boldsymbol{y}^i$ at the previous time point $t_i = t_{i+1} - dt$. Then we denote by $\boldsymbol{y}_j^{i+1}$ the j-th iteration of the

fixed point method. We therefore treat the left-hand side of (73c)-(73d) implicitly, while we evaluate the right-hand side at the attempt solution $\boldsymbol{y}_j^{i+1}$. We can therefore discretise the problem, which reduces to the solving the linear system:

$$A(\boldsymbol{y}^i)\boldsymbol{y}_{j+1}^{i+1} = \boldsymbol{b}(\boldsymbol{y}^i, \boldsymbol{y}_j^i), \tag{74}$$

where the dependency of the vector $\boldsymbol{b}$ on $\boldsymbol{y}^i$ comes from the governing equation, while the dependency on $\boldsymbol{y}_j^i$ from the boundary condition. We therefore iterate over j until the difference between two iteration is less than the tolerance $\|\boldsymbol{y}_{j+1}^i - \boldsymbol{y}_j^i\| < toll$. If the number of step required to match the tolerance is above a set limit N_{max} then the time step dt is decreased. We also add an extra check on the solution to make sure that the volume fraction ϕ_s, ϕ_+ and ϕ_n (which can be evaluated from the other two) have values between 0 and 1. If this is not the case, the time step dt is decreased.

References

[1] T. Bertrand, J. Peixinho, S. Mukhopadhyay, and C. W. MacMinn. Dynamics of swelling and drying in a spherical gel. *Physical Review Applied*, 6(6):064010, 2016.

[2] D. Buenger, F. Topuz, and J. Groll. Hydrogels in sensing applications, dec 2012.

[3] G. Celora, M. G. Hennessy, A. Münch, B. Wagner, and S. Waters. Asymptotic derivation of jump conditions across a thin debye layer for a polyelectrolyte gel. *Submitted*, 2020.

[4] G. Celora, M. G. Hennessy, A. Münch, B. Wagner, and S. Waters. A kinetic model of a polyelectrolyte gel undergoing phase separation. *Submitted*, 2020.

[5] S. Chaterji, I. K. Kwon, and K. Park. Smart polymeric gels: Redefining the limits of biomedical devices, aug 2007.

[6] M. S. Dimitriyev, Y.-W. Chang, P. M. Goldbart, and A. Fernández-Nieves. Swelling thermodynamics and phase transitions of polymer gels. *Nano Futures*, 3(4):042001, oct 2019.

[7] A. Dobrynin. Theory and simulations of charged polymers: From solution properties to polymeric nanomaterials. *Current Opinion in Colloid & Interface Science*, 13(6):376–388, 2008.

[8] A. D. Drozdov and J. deClaville Christiansen. Modeling the effects of pH and ionic strength on swelling of polyelectrolyte gels. *The Journal of Chemical Physics*, 142(11):114904, 2015.

[9] A. D. Drozdov, A. A. Papadimitriou, J. H. Liely, and C. G. Sanporean. Constitutive equations for the kinetics of swelling of hydrogels. *Mechanics of Materials*, 2016.

[10] K. Dusek and D. Patterson. Transition in swollen polymer networks induced by intramolecular condensation. *Journal of Polymer Science Part A-2: Polymer Physics*, 6(7):1209–1216, 1968.

[11] A. Estévez-Torres and D. Baigl. DNA compaction: Fundamentals and applications. *Soft Matter*, 7(15):6746, 2011.

[12] M. E. Gurtin. Generalized ginzburg-landau and cahn-hilliard equations based on a microforce balance. *Physica D: Nonlinear Phenomena*, 92(3):178 – 192, 1996.

[13] M. G. Hennessy, A. Münch, and B. Wagner. Phase separation in swelling and deswelling hydrogels with a free boundary. *Phys. Rev. E*, 101:032501, Mar 2020.

[14] W. Hong. *Continuum Models of Stimuli-responsive Gels*, pages 165–196. Springer Berlin Heidelberg, Berlin, Heidelberg, 2012.

[15] W. Hong, X. Zhao, and Z. Suo. Large deformation and electrochemistry of polyelectrolyte gels. *Journal of the Mechanics and Physics of Solids*, 58(4):558–577, apr 2010.

[16] F. Horkay, I. Tasaki, and P. J. Basser. Effect of monovalent- divalent cation exchange on the swelling of polyacrylate hydrogels in physiological salt solutions. *Biomacromolecules*, 2(1):195–199, 2001.

[17] J. Hua, M. K. Mitra, and M. Muthukumar. Theory of volume transition in polyelectrolyte gels with charge regularization. *The Journal of Chemical Physics*, 136(13):134901, 2012.

[18] A. R. Khokhlov and E. Y. Kramarenko. Weakly charged polyelectrolytes:âĂĽ collapse induced by extra ionization. *Macromolecules*, 29(2):681–685, 1996.

[19] H. J. Kwon, Y. Osada, and J. P. Gong. Polyelectrolyte gels-fundamentals and applications. *Polymer Journal*, 38(12):1211–1219, nov 2006.

[20] M. P. Lutolf and J. A. Hubbell. Synthetic biomaterials as instructive extracellular microenvironments for morphogenesis in tissue engineering, jan 2005.

[21] E. S. Matsuo and T. Tanaka. Patterns in shrinking gels. *Nature*, 358(6386):482–485, 1992.

[22] J. L. Mccoy and M. Muthukumar. Dynamic light scattering studies of ionic and nonionic polymer gels with continuous and discontinuous volume transitions. *Journal of Polymer Science Part B: Polymer Physics*, 48(21):2193–2206, 2010.

[23] M. Mussel and F. Horkay. Experimental Evidence for Universal Behavior of Ion-Induced Volume Phase Transition in Sodium Polyacrylate Gels. *The Journal of Physical Chemistry Letters*, 10(24):7831–7835, 2019.

[24] C. Ning, Z. Zhou, G. Tan, Y. Zhu, and C. Mao. Electroactive polymers for tissue regeneration: Developments and perspectives, jun 2018.

[25] S. Puri and K. Binder. Surface-directed phase separation with off-critical composition: Analytical and numerical results. *Physical Review E*, 66(6):061602, 2002.

[26] D. Roshal, O. Konevtsova, A. Losdorfer Bozic, and et al. ph-induced morphological changes of proteinaceous viral shells. *Scientific Reports*, 9:5341, 2019.

[27] C. E. Sing, J. W. Zwanikken, and M. Olvera de la Cruz. Effect of ionâĂŞion correlations on polyelectrolyte gel collapse and reentrant swelling. *Macromolecules*, 46(12):5053–5065, 2013.

[28] M. A. Stuart, W. T. Huck, J. Genzer, M. Müller, C. Ober, M. Stamm, G. B. Sukhorukov, I. Szleifer, V. V. Tsukruk, M. Urban, F. Winnik, S. Zauscher, I. Luzinov, and S. Minko. Emerging applications of stimuli-responsive polymer materials. 9(2):101–113, jan 2010.

[29] T. Tanaka. Collapse of gels and the critical endpoint. *Phys. Rev. Lett.*, 40:820–823, Mar 1978.

[30] S.-L. Xue, B. Li, X.-Q. Feng, and H. Gao. A non-equilibrium thermodynamic model for tumor extracellular matrix with enzymatic degradation. *Journal of the Mechanics and Physics of Solids*, 104:32 – 56, 2017.

[31] Y. Yu, C. M. Landis, and R. Huang. Salt-induced swelling and volume phase transition of polyelectrolyte gels. *Journal of Applied Mechanics*, 84(5):051005, 2017.

[32] R. Zandi, B. Dragnea, A. Travesset, and R. Podgornik. On virus growth and form. *Physics Reports*, 847:1–102, 2020.

[33] A. Y. Zubarev, F. A. Blyakhman, G. H. Pollack, P. Gusev, and A. P. Safronov. Self-Similar Wave of Swelling/Collapse Phase Transition along Polyelectrolyte Gel. *Macromolecular Theory and Simulations*, 13(8):697–701, 2004.